DISCRETE DIFFUSION SAMPLERS AND BRIDGES: OFF-POLICY ALGORITHMS AND APPLICATIONS IN LATENT SPACES

Arran Carter[*], **Sanghyeok Choi**[*], **Kirill Tamogashev**[*], **Víctor Elvira & Nikolay Malkin**
University of Edinburgh
Edinburgh, Scotland, United Kingdom
{arran.carter@, k.tamogashev@sms., sanghyeok.choi@, victor.elvira@, nmalkin@}ed.ac.uk

ABSTRACT

Sampling from a distribution $p(x) \propto e^{-\mathcal{E}(x)}$ known up to a normalising constant is an important and challenging problem in statistics. Recent years have seen the rise of a new family of amortised sampling algorithms, commonly referred to as diffusion samplers, that enable fast and efficient sampling from an unnormalised density. Such algorithms have been widely studied for continuous-space sampling tasks; however, their application to problems in discrete space remains largely unexplored. Although some progress has been made in this area, discrete diffusion samplers do not take full advantage of ideas commonly used for continuous-space sampling. In this paper, we propose to bridge this gap by introducing off-policy training techniques for discrete diffusion samplers. We show that these techniques improve the performance of discrete samplers on both established and new synthetic benchmarks. Next, we generalise discrete diffusion samplers to the task of bridging between two arbitrary distributions, introducing data-to-energy Schrödinger bridge training for the discrete domain for the first time. Lastly, we showcase the application of the proposed diffusion samplers to data-free posterior sampling in the discrete latent spaces of image generative models.

1 INTRODUCTION

In this paper, we consider the problem of sampling from a distribution over a discrete space $\mathcal{S} = \{1, \dots, C\}^d$ with probability mass function $p_{\text{target}}(x) = \frac{1}{Z} e^{-\mathcal{E}(x)}$. The energy function $\mathcal{E} : \mathcal{S} \to \mathbb{R}$ can be queried pointwise, but the normalising constant Z is not known and samples from p_{target} cannot tractably be drawn. This is the typical setting in variational (Bayesian) inference, and it also appears in statistical mechanics, where energy-based models over discrete spaces are considered (Ising, 1925; Potts, 1952).

Traditionally, sampling from a distribution defined by an unnormalised density is done using Monte Carlo (MC) methods, which exist both for continuous and discrete spaces. Algorithms for densities defined on a continuous domain include Metropolis-Hastings Markov Chain MC (MCMC; Metropolis et al., 1953), annealed importance sampling Neal (2001), sequential MC Del Moral et al. (2006), adaptive importance sampling Bugallo et al. (2017), Hamiltonian MC Neal et al. (2011), as well as their variations. Their discrete analogues include MCMC on discrete state spaces, such as Metropolis-Hastings and Gibbs sampling, with foundational methodological work by Hastings (1970), Besag (1974), and Geman & Geman (1984), as well as theoretical developments for sampling and approximate counting in combinatorial spaces by Jerrum & Sinclair (1996). Gradient-based MCMC methods in the discrete domain have also been explored Grathwohl et al. (2021); Zhang et al. (2022b).

The popularity of diffusion generative models as approximators for empirical data distributions Sohl-Dickstein et al. (2015); Ho et al. (2020); Song et al. (2021) motivated the adaptation of similar techniques to sampling problems, giving rise to the family of sampling algorithms called *diffusion samplers*. Diffusion samplers (*e.g.*, Zhang & Chen, 2022; Vargas et al., 2023; Richter et al., 2024; Chen et al., 2025a; Albergo & Vanden-Eijnden, 2025) use a diffusion process to model the transition

[*]Equal contribution.

dynamics from a tractable distribution to a target distribution from which samples are not available. Unlike diffusion generative models, which are trained to maximise a variational bound on the likelihood of true samples, diffusion samplers typically optimise a stochastic optimal control Zhang & Chen (2022); Berner et al. (2024) or path-space matching (Richter et al., 2020; Lahlou et al., 2023) objective; see Berner et al. (2026) for unifying theory. These samplers can be further improved by the introduction of off-policy reinforcement learning (RL) techniques to facilitate mode coverage and improve sampling quality (Sendera et al., 2024).

Recently, diffusion samplers have also been adapted for sampling from discrete unnormalised densities Zhu et al. (2025); Holderrieth et al. (2025); Sanokowski et al. (2025a), building upon the discrete diffusion modelling framework established by Hoogeboom et al. (2021); Austin et al. (2021); Campbell et al. (2022). However, these algorithms do not take full advantage of off-policy RL. At the same time, off-policy algorithms equivalent to discrete diffusion samplers were considered as early as Zhang et al. (2022a), but the connection has not been recognised until now. Encouraged by these successes, we make our first contribution:

(1) We introduce off-policy RL methods into the training of discrete diffusion samplers (§2.2) and show their benefits on various established and new tasks (§4.1 and 4.2).

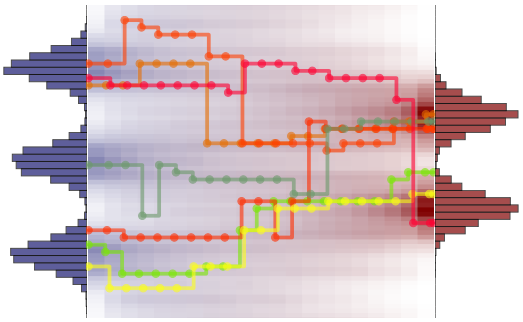

Figure 1: Trajectories sampled from a learnt approximation to the discrete Schrödinger bridge between a mixture of three Gaussians (left, given by samples), and a mixture of two Gaussians (right, given by an unnormalised density), both quantised and represented as 6-bit binary Gray codes. Background shading represents the marginal densities at each step.

We also consider the problem of bridging two arbitrary distributions by finding the Schrödinger bridge (Schrödinger, 1931; 1932), a dynamic version of an optimal transport plan. This problem has been solved for continuous (De Bortoli et al., 2021; Vargas et al., 2021, *inter alia*) and discrete (Kim et al., 2025a; Ksenofontov & Korotin, 2025) cases. However, these solutions consider the setting when samples for both distributions are available – the data-to-data setting. Recently, the problem of finding the Schrödinger bridge between two distributions when one (or both) of them are only given by an unnormalised density function (data-to-energy and energy-to-energy, respectively) was considered by Tamogashev & Malkin (2026). Building upon their work:

(2) We generalise discrete diffusion samplers to data-to-energy Schrödinger bridges (§2.3 and 4.2; Fig. 1).

Previously, evaluation of discrete diffusion samplers has mostly been conducted on synthetic densities. We show, for the first time, that discrete diffusion samplers can enable posterior inference in the discrete latent spaces of pretrained image generative models, forming our third contribution:

(3) We apply discrete diffusion samplers to the problem of sampling posterior distributions in the latent spaces of generative models (§3 and §4.3).

2 Algorithms for discrete diffusion samplers

We now describe the preliminaries (§2.1) and new methods (§2.2) for discrete diffusion sampling. Subsequently, we generalise the sampling problem to the problem of bridging between two arbitrary distributions (§2.3). **Related work** is discussed throughout the text as relevant.

2.1 Setting and preliminaries

The exposition here synthesises the views of discrete diffusion via any-order autoregressive modelling and stochastic optimal control (Austin et al., 2021; Zhu et al., 2025) in a way that makes clear their connection to hierarchical variational inference (Ranganath et al., 2016) and the analogy with the theory for continuous-space diffusion samplers (Berner et al., 2026).

We wish to sample from the discrete state space $\mathcal{S} = \{1, \dots, C\}^d$ of sequences of length d in a vocabulary of size C according to the distribution with probability mass function $p_{\text{target}}(x) = \frac{1}{Z} e^{-\mathcal{E}(x)}$,

where $\mathcal{E} : \mathcal{S} \to \mathbb{R}$ is an energy function. We do not assume knowledge of the normalising constant $Z = \sum_{x \in \mathcal{S}} e^{-\mathcal{E}(x)}$.

Sampling with discrete measure transport. Discrete diffusion models decompose sampling from $\mathcal{S}$ as a Markov chain $X_0 \to X_1 \to \cdots \to X_N$, where each X_n is a random variable taking values in $\mathcal{S}$ or in some extended space $\overline{\mathcal{S}} \supseteq \mathcal{S}$ (for example, in masked diffusion, $\overline{\mathcal{S}} = (\{1, \ldots, C\} \cup \{\star\})^d$, where $\star$ is the mask token). The goal is to find transition kernels[1] $\overrightarrow{p}_\theta(X_{n+1} \mid X_n)$ such that when X_0 is distributed as some known distribution p_0, the marginal distribution over X_N induced by following the kernels for N steps has support only over $\mathcal{S}$ and coincides on $\mathcal{S}$ with the target $p_{\text{target}}(X_N)$.

The initial distribution p_0 and kernels $\overrightarrow{p}_\theta$ determine a distribution over trajectories $X_{0:N} = (X_0, \ldots, X_N)$:

$$(p_0 \otimes \overrightarrow{p}_\theta^{\otimes N})(X_{0:N}) = p_0(X_0) \prod_{n=0}^{N-1} \overrightarrow{p}_\theta(X_{n+1} \mid X_n). \tag{1}$$

Restating the above goal, we aim for the marginal distribution $(p_0 \otimes \overrightarrow{p}_\theta^{\otimes N})(X_N)$ to be equal to $p_{\text{target}}(X_N)$.

In order to set a learning target for the forward kernels $\overrightarrow{p}_\theta$, we define backward (noising) kernels $\overleftarrow{p}(X_n \mid X_{n+1})$, which similarly give a distribution over trajectories

$$(p_{\text{target}} \otimes \overleftarrow{p}^{\otimes N})(X_{0:N}) = p_{\text{target}}(X_N) \prod_{n=0}^{N-1} \overleftarrow{p}(X_n \mid X_{n+1}), \tag{2}$$

where p_{target} is understood to be 0 for elements of $\overline{\mathcal{S}} \setminus \mathcal{S}$.

Learning objectives for discrete diffusion samplers aim to match the two distributions over trajectories (1) and (2) in some measure of divergence. If the two distributions coincide, their marginal distributions over X_N coincide; because $(p_{\text{target}} \otimes \overleftarrow{p}^{\otimes N})(X_N) = p_{\text{target}}(X_N)$ by construction, satisfying this equality achieves the desired goal.

Common choices of $\overleftarrow{p}$. Two common choices for $\overleftarrow{p}$, introduced by Austin et al. (2021), are the uniform diffusion process and the masking process, where each transition $\overleftarrow{p}(X_n \mid X_{n+1})$ replaces the entries at some randomly chosen positions in X_{n+1} by the mask token $\star$ (see §B).

To make it possible to match the forward and reverse distributions, the marginal $(p_{\text{target}} \otimes \overleftarrow{p}^{\otimes N})(X_0)$ should equal $p_0(X_0)$. For example, in the case of masking diffusion, p_0 and the final kernel $\overleftarrow{p}(X_0 \mid X_1)$ both put all mass on the state $(\star, \ldots, \star)$. Similarly, we require that the final kernel $\overrightarrow{p}_\theta(X_N \mid X_{N-1})$ places zero mass on $\overline{\mathcal{S}} \setminus \mathcal{S}$.

We remark that if $\overleftarrow{p}$ masks exactly one entry on each transition, we precisely recover the setting of Zhang et al. (2022a), whose backward policy is used as an auxiliary object in training samplers for energy-based models. Those algorithms, described there in the language of generative flow networks (Bengio et al., 2021; 2023), used trajectory balance ((3) below) and off-policy training (§2.2). It should be noted that this line of work – which draws more from the entropic RL literature (cf. Tiapkin et al. (2024); Deleu et al. (2024)) than from the domain of generative modelling – predates the recent developments in masked discrete diffusion samplers (Zhu et al., 2025), yet the connection has not been recognised.

Objectives. Various loss functions exist to enforce the matching of distributions induced by the forward and backward processes. Those we study are of the second-moment form, depending on a distribution over trajectories $\mathbb{P}$:

$$\mathcal{L}^{\mathbb{P}} = \mathop{\mathbb{E}}_{X_{0:N} \sim \mathbb{P}} \left[\left(\log \frac{(p_0 \otimes \overrightarrow{p}_\theta^{\otimes N})(X_{0:N})}{(p_{\text{target}} \otimes \overleftarrow{p}^{\otimes N})(X_{0:N})} - c \right)^2 \right], \tag{3}$$

where the numerator and denominator are given by (1) and (2), respectively, and c is a scalar that we choose.

[1] We do not explicitly write the dependence on the time step n in the kernel.

Note that while the mass function $p_{\text{target}}(X_N) \propto e^{-\mathcal{E}(X_N)}$ is only known up to a normalising constant, this constant can be additively absorbed into c. Taking c to be a learnt parameter recovers the *trajectory balance* (TB) objective, which was originally introduced for discrete-space sampling in Malkin et al. (2022) and used for a variety of discrete-space sampling problems (Jain et al., 2022; Deleu et al., 2022; van Krieken et al., 2023; Kim et al., 2024, *inter alia*), while taking c to be the value minimising the empirical mean over a batch of samples from $\mathbb{P}$ recovers the *log-variance* (LV) objective, introduced in Richter et al. (2020) and subsequently studied for both continuous-space (Richter et al., 2024; Sendera et al., 2024; Gritsaev et al., 2025; Blessing et al., 2025) and discrete-space diffusion (Holderrieth et al., 2025; Zhu et al., 2025; Guo et al., 2025).

Notably, if $\mathbb{P} = p_0 \otimes \overrightarrow{p}_\theta^{\otimes N}$ (*on-policy objective*), the gradient of $\mathcal{L}^{\mathbb{P}}$ coincides up to a scalar with the gradient of the (reverse) KL divergence for any choice of c (Richter et al., 2020; Malkin et al., 2023; Zimmermann et al., 2023):

$$\nabla_\theta \mathcal{L}^{\mathbb{P}}|_{\mathbb{P}=p_0\otimes\overrightarrow{p}_\theta^{\otimes N}} = 2\nabla_\theta \mathrm{KL}(p_0 \otimes \overrightarrow{p}_\theta^{\otimes N} \,\|\, p_{\text{target}} \otimes \overleftarrow{p}^{\otimes N}).$$

However, the minimiser of (3) for *any* full-support $\mathbb{P}$ is unique and satisfies $p_0 \otimes \overrightarrow{p}_\theta^{\otimes N} = p_{\text{target}} \otimes \overleftarrow{p}^{\otimes N}$, which allows the use of other distributions $\mathbb{P}$, possibly varying over the course of training. The choice of $\mathbb{P}$ is the subject of the next section.

Variable time discretisation. Continuous-time diffusion processes can be sampled with varying time discretisation, effectively modifying the step size in the Euler-Maruyama integration of a stochastic differential equation (Song et al., 2021). Similarly, the continuous-time view of discrete diffusion (Campbell et al., 2022) allows sampling from a denoising process with a larger number of steps than used during training by changing the transition kernel appropriately while keeping the model fixed. Extending the results of Berner et al. (2026) to the discrete-space case, we find that unmasking diffusion samplers trained with few unmasking steps perform well when sampled with one unmasked position per transition; see §B.1 for details.

2.2 Off-policy training strategies

The choice of $\mathbb{P}$ gives rise to two different ways in which to train models: the choice $\mathbb{P} = p_0 \otimes \overrightarrow{p}_\theta^{\otimes N}$ is referred to as "on-policy" training. Off-policy training – that is, a choice of $\mathbb{P}$ that differs from $p_0 \otimes \overrightarrow{p}_\theta^{\otimes N}$ – allows for efficient exploration. Many varieties of off-policy trajectory distributions $\mathbb{P}$ have been considered in the literature on RL for sampling or on generative flow networks, ranging from application-specific heuristic search (Phillips & Cipcigan, 2024; Kim et al., 2024; 2025b) to learnt exploration policies and approximate Bayesian ensembles (Kim et al., 2025c; Rector-Brooks et al., 2023; Muhammad & Lahlou, 2025).

We describe the three off-policy strategies we consider – variations on replay buffer techniques motivated by their successful use in past work – in §A.

2.3 Discrete data-to-energy Schrödinger bridges

The bridge problem is a generalisation of the sampling problem described in the previous sections. Rather than taking p_0 to be a simple, known distribution and choosing $\overleftarrow{p}$ such that $(p_{\text{target}} \otimes \overleftarrow{p}^{\otimes N})(X_0) = p_0(X_0)$ by construction, we take p_0 to be arbitrary and learn $\overleftarrow{p}_\varphi$ as a parametric kernel. The bridge problem seeks a pair of time-dependent kernels $\overrightarrow{p}_\theta$ and $\overleftarrow{p}_\varphi$ that represent the same joint distribution over $X_{0:N}$ transporting p_0 to $p_N = p_{\text{target}}$ and vice versa, *i.e.*, satisfying $p_0 \otimes \overrightarrow{p}_\theta^{\otimes N} = p_{\text{target}} \otimes \overleftarrow{p}_\varphi^{\otimes N}$. (Here, we assume that $\overline{\mathcal{S}} = \mathcal{S}$.)

Among all pairs of kernels that solve the bridge problem, the Schrödinger bridge (SB; Schrödinger, 1931; 1932) is the pair that minimises the KL divergence to some reference distribution $\mathbb{Q}$, assumed to be given by a kernel $\overrightarrow{p}_{\text{ref}}$:[2]

$$(\overrightarrow{p}^*, \overleftarrow{p}^*) = \underset{\substack{(\overrightarrow{p},\overleftarrow{p}):\\ \mathbb{P}:=p_0\otimes\overrightarrow{p}^{\otimes N}=p_{\text{target}}\otimes\overleftarrow{p}^{\otimes N}}}{\arg\min} \mathrm{KL}(\mathbb{P} \,\|\, \mathbb{Q}). \tag{4}$$

[2]Although the SB problem is typically posed as a minimisation over all processes (joint distributions), the solution can be shown to be Markov and thus factorisable into kernels in either direction.

Inverse temp. →	Ising, $\beta = 0.4407$					Ising, $\beta = 0.6$					Ising, $\beta = 1.2$				
Method ↓ Metric →	ELBO ↑	EUBO ↓	Sink. ↓	Mag. ↓	Corr. ↓	ELBO ↑	EUBO ↓	Sink. ↓	Mag. ↓	Corr. ↓	ELBO ↑	EUBO ↓	Sink. ↓	Mag. ↓	Corr. ↓
MH MCMC	-	-	$48.47_{\pm 0.29}$	$0.04_{\pm 0.01}$	$0.14_{\pm 0.01}$	-	-	$8.64_{\pm 0.21}$	$0.09_{\pm 0.06}$	$0.22_{\pm 0.02}$	-	-	$1.05_{\pm 0.21}$	$0.06_{\pm 0.04}$	$0.23_{\pm 0.02}$
MDNS (WDCE)	$237.99_{\pm 0.49}$	$245.66_{\pm 8.30}$	$61.60_{\pm 18.23}$	$0.32_{\pm 0.35}$	$0.23_{\pm 0.26}$	$310.18_{\pm 0.33}$	$341.82_{\pm 38.37}$	$48.71_{\pm 55.25}$	$0.41_{\pm 0.46}$	$0.38_{\pm 0.46}$	$614.42_{\pm 0.00}$	$1192.26_{\pm 94.09}$	$126.27_{\pm 0.90}$	$1.00_{\pm 0.00}$	$1.00_{\pm 0.00}$
LV (on-policy)	$237.89_{\pm 0.16}$	$242.32_{\pm 4.20}$	$53.30_{\pm 11.11}$	$0.67_{\pm 0.10}$	$0.43_{\pm 0.10}$	$309.77_{\pm 0.04}$	$422.53_{\pm 94.60}$	$116.96_{\pm 2.15}$	$0.97_{\pm 0.00}$	$0.95_{\pm 0.00}$	$614.42_{\pm 0.00}$	$1726.06_{\pm 144.71}$	$126.89_{\pm 0.96}$	$1.00_{\pm 0.00}$	$1.00_{\pm 0.00}$
LV + Buffer	$238.21_{\pm 0.24}$	$239.00_{\pm 0.18}$	$47.80_{\pm 0.62}$	$\mathbf{0.03_{\pm 0.02}}$	$0.07_{\pm 0.02}$	$308.55_{\pm 1.36}$	$311.05_{\pm 0.36}$	$4.33_{\pm 0.53}$	$0.40_{\pm 0.30}$	$0.27_{\pm 0.25}$	$\mathbf{615.07_{\pm 0.05}}$	$\mathbf{615.12_{\pm 0.01}}$	$\mathbf{0.02_{\pm 0.00}}$	$\mathbf{0.01_{\pm 0.01}}$	$\mathbf{0.00_{\pm 0.00}}$
LV + Buffer + MCMC	$238.28_{\pm 0.04}$	$238.97_{\pm 0.03}$	$47.34_{\pm 0.90}$	$0.12_{\pm 0.07}$	$0.06_{\pm 0.01}$	$310.18_{\pm 0.24}$	$310.65_{\pm 0.08}$	$3.85_{\pm 0.20}$	$0.14_{\pm 0.13}$	$0.04_{\pm 0.05}$	$614.82_{\pm 0.55}$	$615.16_{\pm 0.09}$	$0.04_{\pm 0.04}$	$0.05_{\pm 0.08}$	$0.01_{\pm 0.02}$
TB (on-policy)	$237.64_{\pm 0.23}$	$249.26_{\pm 9.65}$	$68.79_{\pm 16.84}$	$0.78_{\pm 0.02}$	$0.55_{\pm 0.02}$	$309.79_{\pm 0.00}$	$377.92_{\pm 14.19}$	$117.22_{\pm 0.68}$	$0.97_{\pm 0.00}$	$0.95_{\pm 0.00}$	$614.42_{\pm 0.00}$	$1836.55_{\pm 12.21}$	$127.82_{\pm 0.47}$	$1.00_{\pm 0.00}$	$1.00_{\pm 0.00}$
TB + Buffer	$238.43_{\pm 0.02}$	$238.85_{\pm 0.02}$	$46.44_{\pm 0.67}$	$0.08_{\pm 0.05}$	$0.03_{\pm 0.01}$	$310.42_{\pm 0.03}$	$310.56_{\pm 0.01}$	$3.59_{\pm 0.04}$	$0.04_{\pm 0.02}$	$\mathbf{0.00_{\pm 0.00}}$	$614.75_{\pm 0.30}$	$922.79_{\pm 381.43}$	$50.94_{\pm 62.35}$	$0.42_{\pm 0.47}$	$0.40_{\pm 0.49}$
TB + Buffer + MCMC	$\mathbf{238.48_{\pm 0.01}}$	$\mathbf{238.80_{\pm 0.01}}$	$\mathbf{46.22_{\pm 0.36}}$	$0.04_{\pm 0.02}$	$\mathbf{0.02_{\pm 0.01}}$	$\mathbf{310.43_{\pm 0.01}}$	$\mathbf{310.55_{\pm 0.01}}$	$\mathbf{3.47_{\pm 0.12}}$	$\mathbf{0.02_{\pm 0.01}}$	$\mathbf{0.00_{\pm 0.00}}$	$615.03_{\pm 0.06}$	$615.14_{\pm 0.02}$	$\mathbf{0.02_{\pm 0.00}}$	$0.03_{\pm 0.01}$	$\mathbf{0.00_{\pm 0.00}}$

Table 1: Experimental results on 16 × 16 Ising (above) and Potts (right) models (mean±std over 5 runs), showing that off-policy methods deliver consistent improvements.

Inverse temp. →	Potts, $q = 3, \beta = 1.005$					Potts, $q = 3, \beta = 1.2$				
Method ↓ Metric →	ELBO ↑	EUBO ↓	Sink. ↓	Mag. ↓	Corr. ↓	ELBO ↑	EUBO ↓	Sink. ↓	Mag. ↓	Corr. ↓
MH MCMC	-	-	$90.36_{\pm 1.10}$	$\mathbf{0.03_{\pm 0.01}}$	$0.18_{\pm 0.01}$	-	-	$47.27_{\pm 1.29}$	$\mathbf{0.03_{\pm 0.01}}$	$0.28_{\pm 0.00}$
MDNS (WDCE)	$530.03_{\pm 0.60}$	$534.32_{\pm 5.39}$	$84.78_{\pm 10.15}$	$0.08_{\pm 0.06}$	$\mathbf{0.01_{\pm 0.00}}$	$620.23_{\pm 0.52}$	$680.52_{\pm 53.78}$	$99.95_{\pm 70.52}$	$0.58_{\pm 0.46}$	$0.01_{\pm 0.00}$
LV (on-policy)	$529.29_{\pm 0.16}$	$556.12_{\pm 6.21}$	$136.86_{\pm 7.12}$	$0.81_{\pm 0.01}$	$0.07_{\pm 0.01}$	$619.82_{\pm 0.10}$	$748.31_{\pm 70.53}$	$156.71_{\pm 2.69}$	$0.95_{\pm 0.00}$	$\mathbf{0.00_{\pm 0.00}}$
LV + Buffer	$529.26_{\pm 0.70}$	$532.20_{\pm 0.41}$	$83.32_{\pm 1.92}$	$0.04_{\pm 0.03}$	$0.08_{\pm 0.02}$	$619.47_{\pm 1.00}$	$628.47_{\pm 13.62}$	$32.88_{\pm 29.09}$	$0.21_{\pm 0.17}$	$0.02_{\pm 0.01}$
LV + Buffer + MCMC	$528.84_{\pm 1.07}$	$532.45_{\pm 0.64}$	$84.58_{\pm 1.02}$	$0.04_{\pm 0.03}$	$0.09_{\pm 0.02}$	$619.38_{\pm 1.17}$	$621.60_{\pm 0.15}$	$19.56_{\pm 5.21}$	$0.13_{\pm 0.10}$	$0.02_{\pm 0.02}$
TB (on-policy)	$529.06_{\pm 0.18}$	$573.71_{\pm 14.83}$	$143.51_{\pm 4.51}$	$0.81_{\pm 0.02}$	$0.07_{\pm 0.02}$	$619.34_{\pm 0.41}$	$1117.43_{\pm 235.46}$	$161.78_{\pm 3.45}$	$0.96_{\pm 0.01}$	$0.01_{\pm 0.01}$
TB + Buffer	$530.51_{\pm 0.09}$	$531.43_{\pm 0.08}$	$78.89_{\pm 0.98}$	$\mathbf{0.03_{\pm 0.02}}$	$0.02_{\pm 0.01}$	$619.84_{\pm 0.03}$	$705.56_{\pm 16.57}$	$156.12_{\pm 2.14}$	$0.95_{\pm 0.00}$	$\mathbf{0.00_{\pm 0.00}}$
TB + Buffer + MCMC	$\mathbf{530.65_{\pm 0.04}}$	$\mathbf{531.31_{\pm 0.03}}$	$\mathbf{78.50_{\pm 0.83}}$	$\mathbf{0.03_{\pm 0.02}}$	$\mathbf{0.01_{\pm 0.01}}$	$\mathbf{620.73_{\pm 0.15}}$	$\mathbf{621.30_{\pm 0.08}}$	$\mathbf{12.37_{\pm 0.82}}$	$\mathbf{0.03_{\pm 0.02}}$	$\mathbf{0.00_{\pm 0.00}}$

The SB problem has been studied in the case where samples from both p_0 and p_N are available, both in the continuous-space (De Bortoli et al., 2021; Vargas et al., 2021; Chen et al., 2021; 2022; Shi et al., 2023) and discrete-space (Kim et al., 2025a; Ksenofontov & Korotin, 2025) cases. Recently, Tamogashev & Malkin (2026) developed a SB algorithm for the setting where there are no samples available from p_N and only an energy function is given. This algorithm is an adaptation of the iterative proportional fitting procedure (IPF; Fortet, 1940; Kullback, 1968; Chen et al., 2021), studied in the data-to-data case by De Bortoli et al. (2021); Vargas et al. (2021), that uses off-policy objectives similar to those described in §2.1 and 2.2. This adaptation was studied for the continuous state space setting; here we investigate its extension into discrete state spaces.

IPF alternately fits joint distributions $\overrightarrow{\mathbb{P}}$ and $\overleftarrow{\mathbb{P}}$. Initialising $\overrightarrow{\mathbb{P}}^0 = \mathbb{Q}$, we iteratively solve:

$$\overleftarrow{\mathbb{P}}^{k+1} = \underset{\overleftarrow{\mathbb{P}} : \overleftarrow{\mathbb{P}}(X_0) = p_0(X_0)}{\arg\min} \quad \mathrm{KL}(\overleftarrow{\mathbb{P}} \mid \overrightarrow{\mathbb{P}}^k) \tag{5a}$$

$$\overrightarrow{\mathbb{P}}^{k+1} = \underset{\overrightarrow{\mathbb{P}} : \overrightarrow{\mathbb{P}}(X_N) = p_N(X_N)}{\arg\min} \quad \mathrm{KL}(\overrightarrow{\mathbb{P}} \mid \overleftarrow{\mathbb{P}}^{k+1}) \tag{5b}$$

for $k = 0, 1, 2, \ldots$. As $k \to \infty$, the two processes can be shown to converge (in the KL sense) to the solution of (4). The solution at each iteration is Markov, and we assume $\overrightarrow{\mathbb{P}}^k$, $\overleftarrow{\mathbb{P}}^k$ to be represented by kernels $\overrightarrow{p}^k$, $\overleftarrow{p}^k$, respectively.

Choosing a parametric representation of the kernels, denoted $\overrightarrow{p}^k_\theta$, $\overleftarrow{p}^k_\varphi$, the optimisation problems in (5) can be solved approximately. When samples from p_0 are available, (5a) can be solved by maximum-likelihood training. However, when samples from p_N are not available, (5b) features the problem of exploration of p_{target} and requires a variant of the log-variance loss (see Tamogashev & Malkin, 2026, equation (8), for derivation). This objective can be directly translated to our discrete-space setting, and the full algorithm is detailed in Algorithm 2.

3 Outsourced samplers and bridges in discrete latent spaces

Conditioning a pretrained model is a fundamental problem of generative modelling. Conditional sampling can be formulated as posterior inference: given a pretrained model $p(x)$ and a condition $p(y \mid x)$ – such as the likelihood under a classifier of x belonging to class y – the goal is to sample from the posterior $p(x \mid y) \propto p(x)p(y \mid x)$ without observing any unbiased conditional samples.

If the prior $p(x)$ can be expressed as the pushforward by a function f of a random noise variable $z \sim p_{\text{latent}}(z)$[3], then the posterior sampling problem is equivalent to sampling z from $p(z \mid y) \propto p_{\text{latent}}(z)p(y \mid f(z))$. The samples $f(z)$ for $z \sim p(z \mid y)$ then follow the posterior $p(x \mid y)$. This observation was used by Venkatraman et al. (2025), who proposed to train diffusion samplers of posteriors $p(z \mid y)$ in the (continuous) latent spaces of various generative models, such as VAEs, GANs, and continuous normalising flows. Such an approach to posterior inference does not require evaluating the density of $p(x)$ or differentiating through f. (Alternative methods for drawing samples from $p(z \mid y)$, also using this *noise outsourcing* principle, were proposed in Tang et al. (2025); Wang et al. (2025); Kalaivanan et al. (2025); Om et al. (2025).)

[3]That is, if $z \sim p_{\text{latent}}(z)$ and $x = f(z)$, then $x \sim p(x)$.

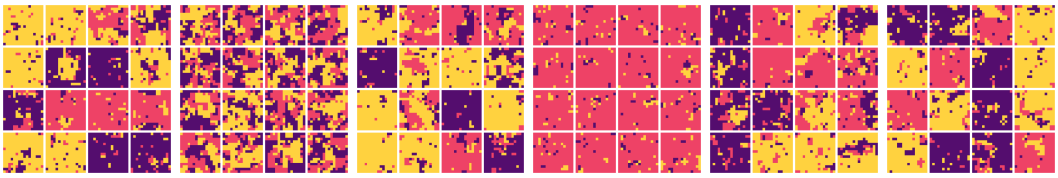

Ground Truth | MH | MDNS | TB (on-policy) | TB + Buffer | TB + Buffer + MCMC

Figure 2: Samples generated by each method for the 16×16 Potts model with $\beta = 1.005$.

Table 2: Experimental results on discretised synthetic densities (mean±std over 5 runs).

Target →	40GMM ($d = 2 \times 8 = 16$)				40GMM ($d = 4 \times 8 = 32$)				ManyWell ($d = 4 \times 8 = 32$)				ManyWell ($d = 10 \times 8 = 80$)			
Method ↓ Metric →	ELBO ↑	EUBO ↓	MMD ↓	Sink. ↓	ELBO ↑	EUBO ↓	MMD ↓	Sink. ↓	ELBO ↑	EUBO ↓	MMD ↓	Sink. ↓	ELBO ↑	EUBO ↓	MMD ↓	Sink. ↓
MH MCMC	-	-	**0.01±0.00**	**0.04±0.00**	-	-	0.05±0.00	4.86±8.49	-	-	**0.01±0.00**	**0.04±0.00**	-	-	**0.01±0.00**	**1.06±0.01**
MDNS (WDCE)	-17.30±1.76	1.54±0.07	0.03±0.01	0.66±0.05	-16.66±2.25	14.02±1.50	0.17±0.04	349.31±69.18	18.21±0.14	21.44±0.02	0.03±0.01	0.11±0.00	41.52±0.65	54.16±0.14	0.04±0.01	1.82±0.05
LV (on-policy)	**-1.28±0.06**	15.11±1.36	0.23±0.06	144.02±77.54	-2.56±0.27	77.96±13.03	0.42±0.09	2265.84±685.58	**20.18±0.02**	21.43±0.02	0.04±0.01	0.06±0.00	**49.10±0.04**	57.40±0.26	0.14±0.01	1.34±0.02
LV + Buffer	-10.24±1.23	1.15±0.05	0.04±0.01	0.49±0.03	-2.68±0.19	49.77±11.95	0.38±0.10	1566.19±596.76	19.40±0.03	21.03±0.01	0.03±0.00	0.08±0.00	44.83±0.41	54.29±0.08	0.05±0.01	1.83±0.07
LV + Buffer + MCMC	-10.30±1.30	1.18±0.05	0.04±0.01	0.49±0.02	-12.39±2.53	13.25±1.48	0.65±0.05	1070.42±499.38	19.30±0.08	21.03±0.01	0.03±0.01	0.08±0.00	41.80±0.22	54.52±0.07	0.08±0.01	2.23±0.03
TB (on-policy)	-1.29±0.07	14.99±1.52	0.24±0.06	156.58±105.97	**-2.47±0.30**	71.53±7.55	0.40±0.07	2142.65±637.28	**20.18±0.02**	21.43±0.02	0.04±0.00	0.06±0.00	49.05±0.05	57.48±0.28	0.15±0.02	1.37±0.02
TB + Buffer	-3.99±0.12	**0.64±0.01**	0.02±0.01	0.37±0.01	-5.97±1.06	4.20±1.39	0.07±0.03	114.11±53.48	19.80±0.04	**20.93±0.01**	0.02±0.01	0.06±0.00	48.79±0.07	53.18±0.03	0.03±0.01	1.30±0.01
TB + Buffer + MCMC	-3.84±0.15	**0.64±0.03**	0.03±0.01	0.35±0.02	-7.13±0.73	**0.91±0.03**	**0.04±0.01**	**4.25±0.30**	19.72±0.05	**20.93±0.01**	0.02±0.01	0.07±0.00	48.74±0.10	**52.84±0.02**	0.04±0.01	1.36±0.02

Generalising the setup introduced in Venkatraman et al. (2025) to discrete latent spaces, we can train diffusion samplers to model the Bayesian posterior distribution $p(z \mid y)$ in the latent space of a pretrained VQ-VAE model Van Den Oord et al. (2017) with autoregressive prior $p_{\text{latent}}(z)$, which is a model over token sequences of fixed length. One could similarly model Schrödinger bridges between posterior distributions in latent space defined in this way.

4 Experiments

We evaluate the off-policy sampler training strategies (§2.2) and their Schrödinger bridge generalisation (§2.3), on synthetic densities in §4.1 and 4.2 and on outsourced sampling (§3) in §4.3.

Modelling setting: sampling. We train discrete diffusion samplers $\overrightarrow{p}_\theta$ under a masking noising kernel $\overleftarrow{p}$ (details in §B.1). This setup coincides with that formulated in the stochastic optimal control setting by MDNS (Zhu et al., 2025), which primarily used the weighted denoising cross entropy (WDCE) loss for high-dimensional problems and only considered a masking kernel $\overleftarrow{p}$ that masks one entry per step. In contrast, we allow for multiple maskings per step in $\overleftarrow{p}$ (and correspondingly multiple unmaskings in $\overrightarrow{p}_\theta$). As known from the literature on discrete diffusion models trained on target data (Hayakawa et al., 2025; Chen et al., 2025b), this introduces correlation error, but increases computational speed and eases memory requirements for many choices of loss function. We use the methods of MDNS as our main baseline to which we compare second-moment divergences optimised by both on- and off-policy methods on synthetic targets. We compare samplers trained with TB and LV objectives (§2.1), either with on-policy training or with some combination of the importance-weighted buffer and MCMC exploration strategies from §2.2. We include results for a (learning-free) Metropolis-Hastings algorithm for comparison to the MDNS baseline and to the samplers we study.

Modelling setting: bridges. Masked diffusion does not apply to Schrödinger bridges. Instead, we take a uniform diffusion process (Austin et al. (2021), see §B.2), as the reference kernel $\overrightarrow{p}_{\text{ref}}$.

4.1 Ising and Potts models

The **Potts model** Potts (1952) is an energy-based model from statistical mechanics, defined over a space of *spin states* – discrete variables taking values in $\{1, \ldots, q\}$. We consider spins spatially arranged in an $L \times L$ toroidal lattice, so the state space is $\mathcal{S} = \{1, \ldots, q\}^{L \times L}$.

The energy function depends on a spin interaction coefficient, which we take to be 1 by default. The energy and probability mass functions are then

$$H(x) = -J \sum_{i \sim j} \mathbf{1}_{x_i = x_j}, \quad p_{\text{target}}(x) \propto e^{-\beta H(x)}, \tag{6}$$

where $\beta \in \mathbb{R}^+$ is the inverse temperature and $i \sim j$ denotes that coordinates i and j are adjacent. When J is positive, the energy model favours configurations in which adjacent spins coincide and has q modes, each corresponding to a state with all spins equal. The standard **Ising model** (Ising, 1925) is a special case of the Potts model with $q = 2, J = \frac{1}{2}$.

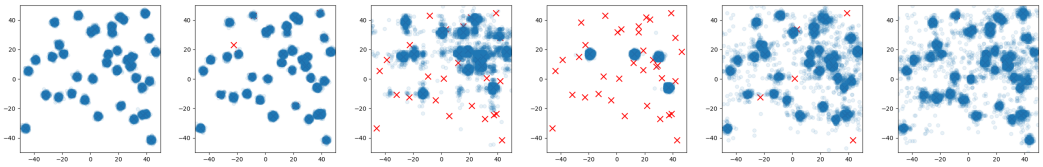

Ground Truth | MH | MDNS | TB (on-policy) | TB + Buffer | TB + Buffer + MCMC

Figure 3: Visualisation of samples generated by each method for the discretised 40GMM ($d = 4 \times 8 = 32$), projected to the first two dimensions. The crosses are placed at the 40 modes of the mixture. Only the off-policy TB + Buffer + MCMC discovers all 40 modes.

We train discrete diffusion samplers on the target energies of Potts and Ising models with $L = 16$ and vary the inverse temperature β to control the difficulty of the problem – a larger β (lower temperature) can lead to more difficult and less stable learning, often collapsing to a single mode. Following Zhu et al. (2025), we report the empirical magnetisation and correlation errors as defined in §D.1, as well as the Sinkhorn distance between approximate and true samples, the ELBO, and the EUBO (Blessing et al., 2024). The correlation error, Sinkhorn, and EUBO metrics require access to true samples, which were obtained from a long-run MCMC chain.

The off-policy methods with MCMC use the Swendsen-Wang algorithm (Swendsen & Wang, 1986; 1987) as a proposal tailored to the structure of this energy model. We note, however, that the MCMC used for exploration during training is not run for sufficiently long for the chains to converge. For a comparison of off-policy methods trained instead with a H-Hamming-ball proposal MH, see §E.1.3. For all other experiment details, see §D.1.

Results. The results on Ising models in Table 1 (top) show that the off-policy methods consistently outperform or match on-policy methods and that TB performs slightly better than LV on most temperatures. The greatest difference between on-policy and off-policy methods occurs at the highest inverse temperatures, as can be visually seen in Figs. 6 and 7 in §E.2.1. In the lowest-temperature setting ($\beta = 1.2$), we see that many of the methods experience severe mode collapse, however, both MCMC-assisted methods successfully manage to model the distribution well.

Table 1 (right) shows results on the Potts model with $q = 3$. The TB off-policy methods outperform both on-policy methods, as well as LV and MDNS. At the lowest temperature ($\beta = 1.2$), many of the methods collapse to a single mode, while both MCMC-assisted methods do not, samples from the Potts model with $\beta = 1.005$ and $\beta = 1.2$ can be seen in Figs. 2 and 8 respectively. Interestingly, for both Ising and Potts models, TB without MCMC is sometimes unstable at low temperatures.

4.2 Discretised synthetic densities

As challenging densities with entangled variables, we consider distributions over $\mathbb{R}^D$, which are converted to distributions over *binary* codes of length $d = 8D$ by subsampling each dimension at 2^8 equally spaced values and representing each resulting coordinate by a Gray code (Gray (1953), §D.2). Such a setting was previously considered for discrete probabilistic modelling in Dai et al. (2020); Zhang et al. (2022a), but not for the problem of sampling a given energy-based model.

We make use of two common synthetic densities for continuous sampling problems, ManyWell ($D = 4$ or 10, a sum of bivariate fourth-degree polynomial energies with 2^D modes; Noé et al. (2019)) and 40GMM ($D = 2$ or 4, a mixture of 40 Gaussians; Midgley et al. (2023)). These continuous-space densities are highly multimodal and challenging to approximate, even with algorithms that assume access to the energy gradient.The off-policy MCMC methods use Metropolis-Hastings with a 1-Hamming-ball proposal; see §D.1.

Diffusion samplers. We study the performance of discrete diffusion samplers with and without off-policy training methods. We use target distribution temperature annealing for all sampling methods and synthetic targets; we investigate the situation where no target annealing is applied in §E.1.1. For evaluation, we use the ELBO and EUBO metrics, as well as the sample-based Sinkhorn and MMD with RBF kernel. See §D.2 for algorithm details.

Table 2 shows performance metrics over all methods considered. The off-policy methods trained with the TB objective consistently outperform or match on-policy methods and other learning-based methods (LV, MDNS) in all metrics. Similar to what was seen in the Ising and Potts models, this improvement is most noticeable on challenging and highly multimodal problems such as the 4-dimensional 40GMM (32-dimensional binary code), where standard on-policy methods fail to

effectively capture all modes of the distribution, as can be seen from Fig. 3 and Fig. 9 in §E.2.2. We further use this task to study more closely the effect of off-policy training; see §E.1.2.

Schrödinger bridges. We investigate our algorithms' ability to construct discrete stochastic transport maps between various pairs of distributions in two dimensions, discretised to 16-dimensional binary Gray codes. In each pair, the first distribution is given by samples and the second by its energy. In Fig. 10 we show samples from the final bridges trained using IPF on three different problems. We compare performance of both on-policy and off-policy methods. While both methods succeed in fitting bridges between simple densities, the off-policy method scales better to the multimodal 40GMM target distribution, where the on-policy sampler collapses. See §D.3 for experimental details.

4.3 Outsourced sampling

We show that discrete diffusion samplers can be used for posterior sampling in the latent spaces of generative models. We chose our generative model to be a VQ-VAE trained on MNIST (Deng, 2012) with 16-dimensional latent space and 8-word codebook ($\mathcal{S} = \{1, \ldots, 8\}^{16}$) using the algorithm in Hu et al. (2023), which allows joint learning of an autoregressive prior $p_{\text{latent}}(z)$ and decoder, whose predicted mean we treat as a deterministic decoding $x = f(z)$. In these experiments, the likelihood function $p(y \mid x)$ returns the probability that the generated image x represents a digit class that is *odd*, *even*, or equal to some number.

In Fig. 4 we show images generated by our approach with both on-policy and off-policy training, showing that both are able to produce digits of the desired classes. Additional images, using different objectives and model architectures, are shown in §E.2.3.

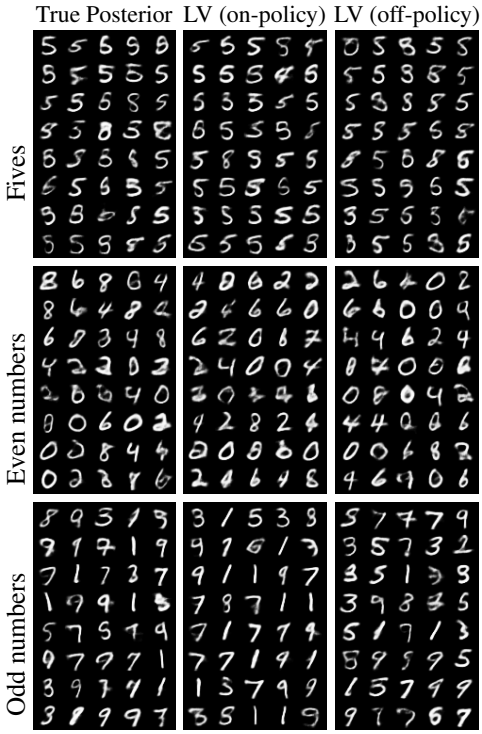

Figure 4: Decoded samples from the true posterior and from diffusion samplers (trained on- and off-policy) in the latent space of a VQ-VAE trained on MNIST. Outsourced discrete diffusion samplers successfully allow conditioning by learning to sample in latent space.

5 Conclusion

We have shown that using off-policy RL methods in training can significantly improve the performance of discrete diffusion samplers. We have demonstrated this in our evaluation on previously considered densities and on more challenging discrete problems, where mode collapse is a concern. We have illustrated, for the first time, discrete Schrödinger bridges in the case where one distribution is given by an energy function and have further tested the capabilities of discrete diffusion samplers on the novel application of posterior sampling in discrete latent spaces.

The methods studied here have certain limitations. Some of these limitations are inherited from the discrete diffusion sampling framework itself, such as the need to fix a noising kernel (which can be alleviated by bridge models or otherwise learning the noising kernel, as was recently shown to be beneficial in continuous spaces by Gritsaev et al. (2025); Sanokowski et al. (2025b)). Others are related to the computational cost of rolling out and storing trajectories; our finding that discrete diffusion samplers can be trained at coarser time scales than those at which they are sampled (and thus at lower cost) begs for an extension of Berner et al. (2026)'s theory regarding the continuous-time limit of diffusion samplers to the discrete-space case.

Beyond the resolution of these limitations, we can identify three practical directions for future work. First, the capabilities of discrete diffusion samplers could be evaluated on problems involving learning an energy function from a dataset (as studied by Zhang et al. (2022a) using methods that are a special case of those we consider). Second, while our work has made a step in improving discrete diffusion samplers, they have yet to be scaled to large problems, such as outsourced sampling for large image generative models, where continuous-space diffusion samplers have been successful (Venkatraman et al., 2025). Third, the potential and applications of Schrödinger bridge algorithms, particularly in latent spaces, for data-free alignment of distributions have yet to be fully understood.

ACKNOWLEDGEMENTS

The work of AC is supported by the UKRI EPSRC through the CDT in Machine Learning Systems hosted in the School of Informatics, University of Edinburgh (EP/Y03516X/1), as well as joint sponsorship from Level E Research. The work of SC, VE, and NM is supported by the Advanced Research and Invention Agency (ARIA). NM acknowledges support from the CIFAR Learning in Machines and Brains programme.

This work was enabled by the computational resources of the Edinburgh International Data Facility (EIDF) and Edinburgh Generative AI Laboratory (GAIL).

REFERENCES

Tara Akhound-Sadegh, Jarrid Rector-Brooks, Avishek Joey Bose, Sarthak Mittal, Pablo Lemos, Cheng-Hao Liu, Marcin Sendera, Siamak Ravanbakhsh, Gauthier Gidel, Yoshua Bengio, Nikolay Malkin, and Alexander Tong. Iterated denoising energy matching for sampling from Boltzmann densities. *International Conference on Machine Learning (ICML)*, 2024.

Tara Akhound-Sadegh, Jungyoon Lee, Avishek Joey Bose, Valentin De Bortoli, Arnaud Doucet, Michael M Bronstein, Dominique Beaini, Siamak Ravanbakhsh, Kirill Neklyudov, and Alexander Tong. Progressive inference-time annealing of diffusion models for sampling from boltzmann densities. *Neural Information Processing Systems (NeurIPS)*, 2025.

Michael S. Albergo and Eric Vanden-Eijnden. NETS: A non-equilibrium transport sampler. *International Conference on Machine Learning (ICML)*, 2025.

Jacob Austin, Daniel D Johnson, Jonathan Ho, Daniel Tarlow, and Rianne Van Den Berg. Structured denoising diffusion models in discrete state-spaces. *Neural Information Processing Systems (NeurIPS)*, 2021.

Emmanuel Bengio, Moksh Jain, Maksym Korablyov, Doina Precup, and Yoshua Bengio. Flow network based generative models for non-iterative diverse candidate generation. *Neural Information Processing Systems (NeurIPS)*, 2021.

Yoshua Bengio, Salem Lahlou, Tristan Deleu, Edward J. Hu, Mo Tiwari, and Emmanuel Bengio. GFlowNet foundations. *Journal of Machine Learning Research (JMLR)*, 24(210):1–55, 2023.

Julius Berner, Lorenz Richter, and Karen Ullrich. An optimal control perspective on diffusion-based generative modeling. *Transactions on Machine Learning Research (TMLR)*, 2024.

Julius Berner, Lorenz Richter, Marcin Sendera, Jarrid Rector-Brooks, and Nikolay Malkin. From discrete-time policies to continuous-time diffusion samplers: Asymptotic equivalences and faster training. *Transactions on Machine Learning Research (TMLR)*, 2026.

Julian Besag. Spatial interaction and the statistical analysis of lattice systems. *Journal of the Royal Statistical Society: Series B (Methodological)*, 36(2):192–225, 1974.

Denis Blessing, Xiaogang Jia, Johannes Esslinger, Francisco Vargas, and Gerhard Neumann. Beyond ELBOs: A large-scale evaluation of variational methods for sampling. *International Conference on Machine Learning (ICML)*, 2024.

Denis Blessing, Julius Berner, Lorenz Richter, and Gerhard Neumann. Underdamped diffusion bridges with applications to sampling. *International Conference on Learning Representations (ICLR)*, 2025.

Monica F Bugallo, Víctor Elvira, Luca Martino, David Luengo, Joaquin Miguez, and Petar M Djuric. Adaptive importance sampling: the past, the present, and the future. *IEEE Signal Processing Magazine*, 34(4):60–79, 2017. URL https://ieeexplore.ieee.org/abstract/document/7974876.

Andrew Campbell, Joe Benton, Valentin De Bortoli, Tom Rainforth, George Deligiannidis, and Arnaud Doucet. A continuous time framework for discrete denoising models. *Neural Information Processing Systems (NeurIPS)*, 2022.

Junhua Chen, Lorenz Richter, Julius Berner, Denis Blessing, Gerhard Neumann, and Anima Anandkumar. Sequential controlled Langevin diffusions. *International Conference on Learning Representations (ICLR)*, 2025a.

Sitan Chen, Kevin Cong, and Jerry Li. Optimal inference schedules for masked diffusion models. *arXiv preprint arXiv:2511.04647*, 2025b.

Tianrong Chen, Guan-Horng Liu, and Evangelos A. Theodorou. Likelihood training of Schrödinger bridge using forward-backward SDEs theory. *International Conference on Learning Representations (ICLR)*, 2022.

Yongxin Chen, Tryphon T Georgiou, and Michele Pavon. Optimal transport in systems and control. *Annual Review of Control, Robotics, and Autonomous Systems*, 4(1):89–113, 2021.

Sanghyeok Choi, Sarthak Mittal, Víctor Elvira, Jinkyoo Park, and Nikolay Malkin. Reinforced sequential Monte Carlo for amortised sampling. *arXiv preprint arXiv:2510.11711*, 2025.

Marco Cuturi. Sinkhorn distances: Lightspeed computation of optimal transport. *Neural Information Processing Systems (NIPS)*, 2013.

Hanjun Dai, Rishabh Singh, Bo Dai, Charles Sutton, and Dale Schuurmans. Learning discrete energy-based models via auxiliary-variable local exploration. *Neural Information Processing Systems (NeurIPS)*, 2020.

Valentin De Bortoli, James Thornton, Jeremy Heng, and Arnaud Doucet. Diffusion schrödinger bridge with applications to score-based generative modeling. *Neural Information Processing Systems (NeurIPS)*, 2021.

Pierre Del Moral, Arnaud Doucet, and Ajay Jasra. Sequential Monte Carlo samplers. *Journal of the Royal Statistical Society Series B: Statistical Methodology*, 68(3):411–436, 2006.

Tristan Deleu, António Góis, Chris Emezue, Mansi Rankawat, Simon Lacoste-Julien, Stefan Bauer, and Yoshua Bengio. Bayesian structure learning with generative flow networks. *Uncertainty in Artificial Intelligence (UAI)*, 2022.

Tristan Deleu, Padideh Nouri, Nikolay Malkin, Doina Precup, and Yoshua Bengio. Discrete probabilistic inference as control in multi-path environments. *Uncertainty in Artificial Intelligence (UAI)*, 2024.

Li Deng. The mnist database of handwritten digit images for machine learning research [best of the web]. *IEEE Signal Processing Magazine*, 29(6):141–142, 2012. doi: 10.1109/MSP.2012.2211477.

Robert Fortet. Résolution d'un système d'équations de M. Schrödinger. *Journal de mathématiques pures et appliquées*, 19(1-4):83–105, 1940.

Stuart Geman and Donald Geman. Stochastic relaxation, Gibbs distributions, and the Bayesian restoration of images. *IEEE Transactions on pattern analysis and machine intelligence*, (6): 721–741, 1984.

Will Grathwohl, Kevin Swersky, Milad Hashemi, David Duvenaud, and Chris Maddison. Oops I took a gradient: Scalable sampling for discrete distributions. *International Conference on Machine Learning (ICML)*, 2021.

Frank Gray. Pulse code communication. *US Patent 2,632,058*, 1953.

Arthur Gretton, Karsten M. Borgwardt, Malte J. Rasch, Bernhard Schölkopf, and Alexander Smola. A kernel two-sample test. *Journal of Machine Learning Research (JMLR)*, 13(25):723–773, 2012.

Timofei Gritsaev, Nikita Morozov, Kirill Tamogashev, Daniil Tiapkin, Sergey Samsonov, Alexey Naumov, Dmitry Vetrov, and Nikolay Malkin. Adaptive destruction processes for diffusion samplers. *arXiv preprint arXiv:2506.01541*, 2025.

Nate Gruver, Samuel Stanton, Nathan Frey, Tim GJ Rudner, Isidro Hotzel, Julien Lafrance-Vanasse, Arvind Rajpal, Kyunghyun Cho, and Andrew G Wilson. Protein design with guided discrete diffusion. *Neural Information Processing Systems (NeurIPS)*, 2023.

Wei Guo, Jaemoo Choi, Yuchen Zhu, Molei Tao, and Yongxin Chen. Proximal diffusion neural sampler. *arXiv preprint arXiv:2510.03824*, 2025.

W Keith Hastings. Monte carlo sampling methods using markov chains and their applications. 1970.

Satoshi Hayakawa, Yuhta Takida, Masaaki Imaizumi, Hiromi Wakaki, and Yuki Mitsufuji. Distillation of discrete diffusion through dimensional correlations. *International Conference on Machine Learning (ICML)*, 2025.

Byeongho Heo, Song Park, Dongyoon Han, and Sangdoo Yun. Rotary position embedding for vision transformer. *European Conference on Computer Vision (ECCV)*, 2024.

Jonathan Ho, Ajay Jain, and Pieter Abbeel. Denoising diffusion probabilistic models. *Neural Information Processing Systems (NeurIPS)*, 2020.

Peter Holderrieth, Michael S Albergo, and Tommi Jaakkola. LEAPS: A discrete neural sampler via locally equivariant networks. *International Conference on Machine Learning (ICML)*, 2025.

Emiel Hoogeboom, Didrik Nielsen, Priyank Jaini, Patrick Forr'e, and Max Welling. Argmax flows and multinomial diffusion: Learning categorical distributions. *Neural Information Processing Systems (NeurIPS)*, 2021.

Edward J. Hu, Nikolay Malkin, Moksh Jain, Katie Everett, Alexandros Graikos, and Yoshua Bengio. GFlowNet-EM for learning compositional latent variable models. *International Conference on Machine Learning (ICML)*, 2023.

Xunpeng Huang, Hanze Dong, Yifan Hao, Yi-An Ma, and Tong Zhang. Reverse diffusion Monte Carlo. *International Conference on Learning Representations (ICLR)*, 2024.

Ernst Ising. Beitrag zur theorie des ferromagnetismus. *Zeitschrift für Physik*, 31(1):253–258, 1925.

Moksh Jain, Emmanuel Bengio, Alex Hernandez-Garcia, Jarrid Rector-Brooks, Bonaventure FP Dossou, Chanakya Ajit Ekbote, Jie Fu, Tianyu Zhang, Michael Kilgour, Dinghuai Zhang, et al. Biological sequence design with GFlowNets. *International Conference on Machine Learning (ICML)*, 2022.

Mark Jerrum and Alistair Sinclair. The Markov chain Monte Carlo method: an approach to approximate counting and integration. *Approximation Algorithms for NP-hard problems, PWS Publishing*, 1996.

Adhithyan Kalaivanan, Zheng Zhao, Jens Sjölund, and Fredrik Lindsten. Ess-flow: Training-free guidance of flow-based models as inference in source space. *arXiv preprint arXiv:2510.05849*, 2025.

Hyeonah Kim, Minsu Kim, Sanghyeok Choi, and Jinkyoo Park. Genetic-guided GFlowNets for sample efficient molecular optimization. *Neural Information Processing Systems (NeurIPS)*, 2024.

Jun Hyeong Kim, Seonghwan Kim, Seokhyun Moon, Hyeongwoo Kim, Jeheon Woo, and Woo Youn Kim. Discrete diffusion Schrödinger bridge matching for graph transformation. *International Conference on Learning Representations (ICLR)*, 2025a.

Minsu Kim, Sanghyeok Choi, Hyeonah Kim, Jiwoo Son, Jinkyoo Park, and Yoshua Bengio. Ant colony sampling with GFlowNets for combinatorial optimization. *International Conference on Artificial Intelligence and Statistics (AISTATS)*, 2025b.

Minsu Kim, Sanghyeok Choi, Taeyoung Yun, Emmanuel Bengio, Leo Feng, Jarrid Rector-Brooks, Sungsoo Ahn, Jinkyoo Park, Nikolay Malkin, and Yoshua Bengio. Adaptive teachers for amortized samplers. *International Conference on Learning Representations (ICLR)*, 2025c.

Grigoriy Ksenofontov and Alexander Korotin. Categorical Schrödinger bridge matching. *International Conference on Learning Representations (ICLR)*, 2025.

Solomon Kullback. Probability densities with given marginals. *The Annals of Mathematical Statistics*, 39(4):1236–1243, 1968.

Salem Lahlou, Tristan Deleu, Pablo Lemos, Dinghuai Zhang, Alexandra Volokhova, Alex Hernández-Garcıa, Léna Néhale Ezzine, Yoshua Bengio, and Nikolay Malkin. A theory of continuous generative flow networks. *International Conference on Machine Learning (ICML)*, 2023.

Long-Ji Lin. Self-improving reactive agents based on reinforcement learning, planning and teaching. *Machine Learning*, 8(3–4):293–321, May 1992.

Ilya Loshchilov and Frank Hutter. Decoupled weight decay regularization. *International Conference on Learning Representations (ICLR)*, 2019.

Nikolay Malkin, Moksh Jain, Emmanuel Bengio, Chen Sun, and Yoshua Bengio. Trajectory balance: Improved credit assignment in GFlowNets. *Neural Information Processing Systems (NeurIPS)*, 2022.

Nikolay Malkin, Salem Lahlou, Tristan Deleu, Xu Ji, Edward Hu, Katie Everett, Dinghuai Zhang, and Yoshua Bengio. GFlowNets and variational inference. *International Conference on Learning Representations (ICLR)*, 2023.

Nicholas Metropolis, Arianna W Rosenbluth, Marshall N Rosenbluth, Augusta H Teller, and Edward Teller. Equation of state calculations by fast computing machines. *The journal of chemical physics*, 21(6):1087–1092, 1953.

Laurence Illing Midgley, Vincent Stimper, Gregor NC Simm, Bernhard Schölkopf, and José Miguel Hernández-Lobato. Flow annealed importance sampling bootstrap. *International Conference on Learning Representations (ICLR)*, 2023.

Volodymyr Mnih. Playing atari with deep reinforcement learning. *arXiv preprint arXiv:1312.5602*, 2013.

Sajan Muhammad and Salem Lahlou. Improved exploration in GFlowNets via enhanced epistemic neural networks. *arXiv preprint arXiv:2506.16313*, 2025.

Radford M Neal. Annealed importance sampling. *Statistics and computing*, 11(2):125–139, 2001.

Radford M Neal et al. MCMC using Hamiltonian dynamics. *Handbook of markov chain monte carlo*, 2(11):2, 2011.

Frank Noé, Simon Olsson, Jonas Köhler, and Hao Wu. Boltzmann generators: Sampling equilibrium states of many-body systems with deep learning. *Science*, 365(6457):eaaw1147, 2019.

Nikolas Nüsken and Lorenz Richter. Solving high-dimensional Hamilton–Jacobi–Bellman PDEs using neural networks: perspectives from the theory of controlled diffusions and measures on path space. *Partial Differential Equations and Applications*, 2(4):48, 2021.

Kiyoung Om, Kyuil Sim, Taeyoung Yun, Hyeongyu Kang, and Jinkyoo Park. Posterior inference in latent space for scalable constrained black-box optimization. *arXiv preprint arXiv:2507.00480*, 2025.

Dominic Phillips and Flaviu Cipcigan. MetaGFN: Exploring distant modes with adapted metadynamics for continuous GFlowNets. *arXiv preprint arXiv:2408.15905*, 2024.

R. B. Potts. Some generalized order-disorder transformations. *Mathematical Proceedings of the Cambridge Philosophical Society*, 48(1):106–109, 1952. doi: 10.1017/S0305004100027419.

Rajesh Ranganath, Dustin Tran, and David Blei. Hierarchical variational models. *International Conference on Machine Learning (ICML)*, 2016.

Jarrid Rector-Brooks, Kanika Madan, Moksh Jain, Maksym Korablyov, Cheng-Hao Liu, Sarath Chandar, Nikolay Malkin, and Yoshua Bengio. Thompson sampling for improved exploration in GFlowNets. *arXiv preprint arXiv:2306.17693*, 2023.

Lorenz Richter, Ayman Boustati, Nikolas Nüsken, Francisco J. R. Ruiz, and Ömer Deniz Akyildiz. VarGrad: A low-variance gradient estimator for variational inference. *Neural Information Processing Systems (NeurIPS)*, 2020.

Lorenz Richter, Julius Berner, and Guan-Horng Liu. Improved sampling via learned diffusions. *International Conference on Learning Representations (ICLR)*, 2024.

Severi Rissanen, RuiKang OuYang, Jiajun He, Wenlin Chen, Markus Heinonen, Arno Solin, and José Miguel Hernández-Lobato. Progressive tempering sampler with diffusion. *International Conference on Machine Learning (ICML)*, 2025.

Subham Sahoo, Marianne Arriola, Yair Schiff, Aaron Gokaslan, Edgar Marroquin, Justin Chiu, Alexander Rush, and Volodymyr Kuleshov. Simple and effective masked diffusion language models. *Neural Information Processing Systems (NeurIPS)*, 2024.

Sebastian Sanokowski, Wilhelm Berghammer, Martin Ennemoser, Haoyu Peter Wang, Sepp Hochreiter, and Sebastian Lehner. Scalable discrete diffusion samplers: Combinatorial optimization and statistical physics. *International Conference on Learning Representations (ICLR)*, 2025a.

Sebastian Sanokowski, Lukas Gruber, Christoph Bartmann, Sepp Hochreiter, and Sebastian Lehner. Rethinking losses for diffusion bridge samplers. *Neural Information Processing Systems (NeurIPS)*, 2025b.

Tom Schaul, John Quan, Ioannis Antonoglou, and David Silver. Prioritized experience replay. *International Conference on Learning Representations (ICLR)*, 2016.

Henrik Schopmans and Pascal Friederich. Temperature-annealed boltzmann generators. *International Conference on Machine Learning (ICML)*, 2025.

Erwin Schrödinger. Über die Umkehrung der Naturgesetze. *Sitzungsberichte der Preussischen Akademie der Wissenschaften, Physikalisch-mathematische Klasse*, pp. 144–153, 1931.

Erwin Schrödinger. Sur la théorie relativiste de l'électron et l'interprétation de la mécanique quantique. In *Annales de l'institut Henri Poincaré*, volume 2, pp. 269–310, 1932.

Marcin Sendera, Minsu Kim, Sarthak Mittal, Pablo Lemos, Luca Scimeca, Jarrid Rector-Brooks, Alexandre Adam, Yoshua Bengio, and Nikolay Malkin. Improved off-policy training of diffusion samplers. *Neural Information Processing Systems (NeurIPS)*, 2024.

Max W Shen, Emmanuel Bengio, Ehsan Hajiramezanali, Andreas Loukas, Kyunghyun Cho, and Tommaso Biancalani. Towards understanding and improving GFlowNet training. *International Conference on Machine Learning (ICML)*, 2023.

Jiaxin Shi, Kehang Han, Zhe Wang, Arnaud Doucet, and Michalis Titsias. Simplified and generalized masked diffusion for discrete data. *Neural Information Processing Systems (NeurIPS)*, 2024.

Yuyang Shi, Valentin De Bortoli, Andrew Campbell, and Arnaud Doucet. Diffusion Schrödinger bridge matching. *Neural Information Processing Systems (NeurIPS)*, 2023.

Jascha Sohl-Dickstein, Eric A. Weiss, Niru Maheswaranathan, and Surya Ganguli. Deep unsupervised learning using nonequilibrium thermodynamics. *International Conference on Machine Learning (ICML)*, 2015.

Yang Song, Jascha Sohl-Dickstein, Diederik P Kingma, Abhishek Kumar, Stefano Ermon, and Ben Poole. Score-based generative modeling through stochastic differential equations. *International Conference on Learning Representations (ICLR)*, 2021.

Robert H. Swendsen and Jian-Sheng Wang. Replica monte carlo simulation of spin-glasses. *Phys. Rev. Lett.*, 57:2607–2609, Nov 1986. doi: 10.1103/PhysRevLett.57.2607. URL https://link.aps.org/doi/10.1103/PhysRevLett.57.2607.

Robert H. Swendsen and Jian-Sheng Wang. Nonuniversal critical dynamics in monte carlo simulations. *Phys. Rev. Lett.*, 58:86–88, Jan 1987. doi: 10.1103/PhysRevLett.58.86. URL https://link.aps.org/doi/10.1103/PhysRevLett.58.86.

Kirill Tamogashev and Nikolay Malkin. Data-to-energy stochastic dynamics. *International Conference on Learning Representations (ICLR)*, 2026.

Zhiwei Tang, Jiangweizhi Peng, Jiasheng Tang, Mingyi Hong, Fan Wang, and Tsung-Hui Chang. Inference-time alignment of diffusion models with direct noise optimization. *International Conference on Machine Learning (ICML)*, 2025.

Daniil Tiapkin, Nikita Morozov, Alexey Naumov, and Dmitry Vetrov. Generative flow networks as entropy-regularized RL. *International Conference on Artificial Intelligence and Statistics (AISTATS)*, 2024.

Aaron Van Den Oord, Oriol Vinyals, et al. Neural discrete representation learning. *Neural Information Processing Systems (NeurIPS)*, 2017.

Emile van Krieken, Thiviyan Thanapalasingam, Jakub Tomczak, Frank Van Harmelen, and Annette Ten Teije. A-NeSI: A scalable approximate method for probabilistic neurosymbolic inference. *Neural Information Processing Systems (NeurIPS)*, 2023.

Francisco Vargas, Pierre Thodoroff, Austen Lamacraft, and Neil Lawrence. Solving Schrödinger bridges via maximum likelihood. *Entropy*, 23(9):1134, August 2021.

Francisco Vargas, Will Grathwohl, and Arnaud Doucet. Denoising diffusion samplers. *International Conference on Learning Representations (ICLR)*, 2023.

Francisco Vargas, Shreyas Padhy, Denis Blessing, and Nikolas Nüsken. Transport meets variational inference: Controlled Monte Carlo diffusions. *International Conference on Learning Representations (ICLR)*, 2024.

Siddarth Venkatraman, Mohsin Hasan, Minsu Kim, Luca Scimeca, Marcin Sendera, Yoshua Bengio, Glen Berseth, and Nikolay Malkin. Outsourced diffusion sampling: Efficient posterior inference in latent spaces of generative models. *International Conference on Machine Learning (ICML)*, 2025.

Clement Vignac, Igor Krawczuk, Antoine Siraudin, Bohan Wang, Volkan Cevher, and Pascal Frossard. Digress: Discrete denoising diffusion for graph generation. *International Conference on Learning Representations (ICLR)*, 2023.

Zifan Wang, Alice Harting, Matthieu Barreau, Michael M Zavlanos, and Karl H Johansson. Source-guided flow matching. *arXiv preprint arXiv:2508.14807*, 2025.

Luhuan Wu, Yi Han, Christian Andersson Naesseth, and John P. Cunningham. Reverse diffusion sequential Monte Carlo samplers. *Neural Information Processing Systems (NeurIPS)*, 2025.

Dinghuai Zhang, Nikolay Malkin, Zhen Liu, Alexandra Volokhova, Aaron Courville, and Yoshua Bengio. Generative flow networks for discrete probabilistic modeling. *International Conference on Machine Learning (ICML)*, 2022a.

Qinsheng Zhang and Yongxin Chen. Path integral sampler: a stochastic control approach for sampling. *International Conference on Learning Representations (ICLR)*, 2022.

Ruqi Zhang, Xingchao Liu, and Qiang Liu. A Langevin-like sampler for discrete distributions. *International Conference on Machine Learning (ICML)*, 2022b.

Yuchen Zhu, Wei Guo, Jaemoo Choi, Guan-Horng Liu, Yongxin Chen, and Molei Tao. MDNS: Masked diffusion neural sampler via stochastic optimal control. *Neural Information Processing Systems (NeurIPS)*, 2025.

Heiko Zimmermann, Fredrik Lindsten, Jan-Willem van de Meent, and Christian A. Naesseth. A variational perspective on generative flow networks. *Transactions on Machine Learning Research (TMLR)*, 2023.

A OFF-POLICY TRAINING STRATEGIES

Replay buffer. A replay buffer is a common reinforcement learning technique (Lin, 1992; Mnih, 2013) in which samples drawn from the policy are stored and reused at a later training step. In our setting, following Sendera et al. (2024), we maintain a buffer of sampled states X_N and reuse them by sampling from $\overleftarrow{p}^{\otimes N}$ to produce trajectories to train with. This procedure mixes samples from the current model and from its earlier iterations, which can be particularly useful if the predictive distribution is rapidly changing during the course of training.

Importance-weighted buffer. Instead of simply sampling from the replay buffer with uniform probability for all elements in the buffer, we can assign different sampling probabilities to each buffer element, known as prioritisation Schaul et al. (2016). Such a scheme was considered for amortised samplers by Tiapkin et al. (2024); Shen et al. (2023). Choi et al. (2025) proposed to weight samples by the importance weights w of the trajectories that produced the buffer samples, computed *at the time the samples are added to the buffer* as:

$$w = \frac{e^{-\mathcal{E}(X_N)} \prod_{n=0}^{N-1} \overleftarrow{p}(X_n \mid X_{n+1})}{p_0(X_0) \prod_{n=0}^{N-1} \overrightarrow{p}_\theta(X_{n+1} \mid X_n)}, \tag{7}$$

where $X_{0:N}$ is a trajectory sampled from $p_0 \otimes \overrightarrow{p}_\theta^{\otimes N}$. By using importance-weighted prioritisation, we focus the training onto samples obtained along trajectories that had high target probability mass but which the sampler had a lower probability of producing.

MCMC exploration from the buffer. In addition to relying on the evolving sampler to explore the space, one can use local search techniques, such as Markov chain Monte Carlo (MCMC), to explore p_{target} and guide the training of the sampler to regions of high density. We adapt the methods for continuous diffusion samplers (Sendera et al., 2024) to discrete spaces, although Monte Carlo methods have been combined with amortised sequential samplers in various other ways (Huang et al., 2024; Akhound-Sadegh et al., 2024; Vargas et al., 2024; Choi et al., 2025; Wu et al., 2025).

Specifically, this is done by refining samples from the replay buffer with several steps of an MCMC kernel whose stationary distribution is p_{target} before they are eventually used for training. Because MCMC does not require evaluations of the model, but only of the energy function, it is computationally inexpensive in comparison to sampler rollouts. The MCMC kernel should be chosen appropriately for the target energy (we explore different options on a synthetic example in §4.1 and E.1.3). Algorithm 1 describes the full training procedure.

B NOISING KERNELS FOR DISCRETE DIFFUSION SAMPLERS

B.1 MASKED DIFFUSION SAMPLING

Masked diffusion models (Austin et al., 2021) have being successfully applied to a variety of problems, including language generation (Shi et al., 2024; Sahoo et al., 2024), protein design (Gruver et al., 2023) and graph generation (Vignac et al., 2023). Recent work has shown the stochastic optimal control formulation of masked diffusion in the problem of discrete state space sampling (Zhu et al., 2025), though only the autoregressive single-unmasking case was considered.

Masked diffusion sampling involves appending to our state space a mask token that we denote with $\star$. The non-terminal states in a trajectory then take values in $\overline{\mathcal{S}} = \{\{1, \ldots, C\} \cup \{\star\}\}^d$, with the trajectory value at time N still taking values in $\mathcal{S}$ in order to be able to satisfy the requirement that the terminal marginal equals the target distribution.

Masked diffusion samplers define the initial distribution to be the Dirac delta distribution over the fully masked state $p_0 = \delta_{(\star,\ldots,\star)}$, and define the reverse process as the masking process, where at step $n+1$ we randomly choose k_{n+1}-elements from the set of elements in X_{n+1} not equal to $\star$, and replace them with $\star$.

Define the set of non-mask elements at time n as $\bullet_n = \{i : (X_n)_i \neq \star\}$, following the notational convention of Zhu et al. (2025) we use $X^{I \leftarrow V}$ to denote the operation of replacing the values of all elements of X from some index set $I = \{i_1, i_2, \ldots, i_k\}$, where $i_j \in \{1, \ldots, d\}$, with those from the set $V = \{v_1, v_2, \ldots, v_k\}$ where $v_j \in \overline{\mathcal{S}}$. In equations:

$$(X^{I\leftarrow V})_j = \begin{cases} X_j & j \notin I \\ v_j & j \in I \end{cases}, V = \{v_1, \dots, v_{|I|}\}.$$

$$\overleftarrow{p}(X_n \mid X_{n+1}) = \frac{1}{\binom{|\bullet_{n+1}|}{k_{n+1}}} \mathbf{1}_{X_n = X_{n+1}^{I\leftarrow\{\star,\dots,\star\}}}$$

To learn the forward process we parameterise the forward kernels using a neural network that takes in $X_n \in \overline{\mathcal{S}}$ and outputs a matrix of size $d \times |\mathcal{S}|$ of probabilities summing to 1 along each row – element (i, j) is the probability of element i taking value j at the next step given that element i has been chosen to be unmasked – we then randomly choose the k_{n+1} elements of X_n to be unmasked and sample the corresponding elements of X_{n+1} from the appropriate categorical distribution, keeping all other values the same.

$$\overrightarrow{p}_\theta(X_{n+1} = X_n^{I\leftarrow V} \mid X_n) = \frac{1}{\binom{d-|\bullet_n|}{k_{n+1}}} \prod_{\substack{i\in I \\ v\in V}} f_\theta(X_n)_{i,v} \mathbf{1}_{(X_n)_i = \star}$$

The set $\{k_1, \dots, k_N\}$ we refer to as the masking schedule; its choice can greatly affect performance. We require that $\sum_{n=1}^{N} k_n = d$ so that we go from $X_N \in \mathcal{S}$ to the fully masked state at X_0. Smaller values for the k_n or, correspondingly, a larger N typically yield more accurate results when attempting to model the conditional distributions. Picking all $k_n = 1$, and therefore $N = d$, corresponds to the any-order autoregressive single-unmasking case which can be seen as exact in the sense that there is no error introduced by the process of unmasking multiple, potentially correlated, elements simultaneously. The trade-off here is in terms of algorithmic speed, lower N means fewer function evaluations and gradient calculations. In our experiments we make use of a random masking schedule where at each backward (forward) step we mask (unmask) randomly between $K_{\min}$ and $K_{\max}$ elements.

B.2 Uniform diffusion sampling

Uniform diffusion sampling (Austin et al., 2021) allows us to stay within the target state space $\mathcal{S}$ at all points along the trajectory. This allows its use in the Schrödinger Bridge problem where we bridge between two distributions.

Binary setting. First, for simplicity, we constrain ourselves to the binary state-space setting $\mathcal{S} = \{0, 1\}^d$. Uniform diffusion sampling selects the initial distribution, p_0, to be the uniform distribution over $\mathcal{S}$. In the binary setting the backward process is simply a flipping procedure where each element of the current state is flipped with some probability p_{flip}.

$$\overleftarrow{p}(X_n \mid X_{n+1}) = \prod_{i=1}^{d} p_{\text{flip}}^{|(X_n)_i - (X_{n+1})_i|}.$$

The forward process can then simply be parameterised using a neural network, f_θ, to predict a d-dimensional vector of flipping probabilities.

$$\overrightarrow{p}_\theta(X_{n+1} \mid X_n) = \prod_{i=1}^{d} f_\theta(X_n)_i^{|(X_n)_i - (X_{n+1})_i|}$$

Unlike masked diffusion which guarantees that the noising process ends at the initial distribution, in uniform discrete diffusion sampling it is crucial that appropriately large values for N or p_{flip} are taken such that X_0 is distributed uniformly over $\mathcal{S}$.

Non-binary setting. To extend the previous definition into the state space $\mathcal{S} = \{1, \dots, C\}^d$ we again define the p_0 as the uniform distribution over $\mathcal{S}$. Similarly to the binary setting we also decide whether to change the value of a particular element of the state with some probability p_{flip}, however if we decide to flip some element then it can take $C - 1$ possible values and so we take the uniform distribution over these.

$$\log \overleftarrow{p}(X_n \mid X_{n+1}) = \sum_{i=1}^{d} \mathbf{1}_{(X_n)_i = (X_{n+1})_i} \log(1 - p_{\text{flip}}) + (\mathbf{1}_{(X_n)_i \neq (X_{n+1})_i}) \log \frac{p_{\text{flip}}}{C - 1}$$

The forward process can then be parameterised by a neural network f_θ which outputs a matrix of probabilities corresponding to the next step categorical distributions for each element of the current state, ensuring that the rows of the matrix sum to 1.

C ALGORITHMS

In this section we detail two algorithms we use for training. Algorithm 1 is used for Ising and Potts models, for synthetics tasks, and for outsourced experiments on MNIST. Algorithm 2 is used to learn discrete data-to-energy Schrödinger bridge. Note, that Algorithm 2 details both off-policy and on-policy versions, with modifications required for off-policy training being highlighted in blue.

Algorithm 1 Off-policy training with MCMC exploration

Require: Target energy $\mathcal{E}$, initial distribution p_0, forward and backward kernels $\overrightarrow{p}_\theta$ and $\overleftarrow{p}$, number of epochs N_{epoch}, batch size M, buffers $\mathcal{B}$ and $\mathcal{B}_{\text{MCMC}}$, off-to-on ratio R, MCMC interval I, MCMC num steps L, MCMC sample ratio r.

for $i = 1, \ldots, N_{\text{epoch}}$ **do**
  if $(i-1) \bmod R = 0$ **then** ▷ On-policy sampling
    Sample trajectories $\{x^m_{0:N}\}_{m=1}^M$ from $p_0 \otimes \overrightarrow{p}_\theta^{\otimes N}$ and compute w^m for each $x^m_{0:N}$. ▷ Eq. (7)
    Update buffer, $\mathcal{B} \leftarrow \mathcal{B} \cup \{(x^m_N, w^m)\}_{m=1}^M$.
  else ▷ Off-policy sampling
    Let $M' = \min(\lceil rM \rceil, |\mathcal{B}_{\text{MCMC}}|)$
    Sample $\{x^m\}_{m=1}^{M'}$ from $\mathcal{B}_{\text{MCMC}}$ uniformly, and sample $\{x^{M'+m}\}_{m=1}^{M-M'}$ from $\mathcal{B}$ proportionally to w^m.
    From each x^m, sample backward trajectories $\{x^m_{0:N}\}_{m=1}^M$ using $\overleftarrow{p}^{\otimes N}$.
  end if
  Update θ using $\nabla_\theta \mathcal{L}^{\mathbb{P}}$ given $\{x^m_{0:N}\}_{m=1}^M$. ▷ Eq. (3)
  if $(i-1) \bmod I = 0$ **then** ▷ MCMC exploration
    Sample $\{x^m\}_{m=1}^M$ from $\mathcal{B}$ proportionally to w^m.
    Run M parallel MCMC chains for L steps, each starting from x^m and take the final state of each chain, $\{x^m_L\}_{m=1}^M$.
    Update MCMC buffer, $\mathcal{B}_{\text{MCMC}} \leftarrow \mathcal{B}_{\text{MCMC}} \cup \{x^m_L\}_{m=1}^M$.
  end if
end for

D EXPERIMENTAL DETAILS

D.1 ISING AND POTTS MODELS

D.1.1 TARGETS

Full detail is given in the main text, see (6) for the Potts energy and the following discussion for the special case of the Ising model.

D.1.2 BASELINES

We consider Metropolis-Hastings with H-Hamming-ball proposals and Masked Diffusion Neural Sampler (Zhu et al., 2025), which shares the same sampling process as ours, as baselines for benchmarking on Ising and Potts models. LEAPS (Holderrieth et al., 2025) is another seminal work in discrete diffusion for sampling, but we exclude it from benchmarking due to differences in the sampling process.

Metropolis-Hastings with H-Hamming-ball proposal (MH). H-Hamming-ball MH employs a proposal kernel that samples candidates within a Hamming distance H from the current state. Specifically, a 1-Hamming-ball proposal uniformly chooses an index $i \in \{1, \ldots, d\}$ and replaces x_i with a new value drawn uniformly from $\{1, \ldots, C\} \setminus \{x_i\}$. The H-Hamming-ball proposal applies the 1-Hamming-ball proposal H times sequentially before the Metropolis-Hastings acceptance step.

We use the above H-Hamming-ball MH algorithm as a baseline for the Ising and Potts models. We tuned H over $\{1, 2, 5, 10\}$ and found $H = 1$ to be the best setting across all Ising and Potts

Algorithm 2 Training of data-to-energy discrete Schödinger bridges. Parts used for off-policy training are marked by blue.

Require: Distribution p_0, distribution p_N with queryable density, backward model $\overleftarrow{p}_\varphi$, forward model $\overrightarrow{p}_\theta$ number of epochs $N_{\text{sb_iter}}$, number of trajectories for forward model training K_{traj}, buffers $\mathcal{B}$ and $\mathcal{B}_{\text{MCMC}}$, MCMC num steps L.

for *sb_iter* $= 1, \ldots, N_{\text{sb_iter}}$ **do**
  while *not converged* **do** ▷ Train backward model to maximise log likelihood.
    Sample $\tau = x_{0:N} \sim p_0 \otimes \overrightarrow{p}_\theta^{\otimes N}$;
    Update φ using $\nabla_\varphi \log \overleftarrow{p}_\varphi(\tau \mid x_N)$.
  end while
  if *use off-policy training* **then**
    Sample a batch of $x_N \sim \mathcal{B}$;
    Run MCMC for L steps on x_N, obtaining $x_N^{'}$;
    Update buffer $\mathcal{B}_{\text{MCMC}}$ with samples $x_N^{'}$.
  end if
  while *not converged* **do** ▷ Train forward model using Log Variance divergence.
    if *on-policy* **then**
      $x_0 \sim p_0(x)$, $\tau^{(j)} \sim \overrightarrow{p}_\theta^{\otimes N}(\tau|x_0)$, $\tau = x_{0:N}$ for $1 \leq j \leq K_{\text{traj}}$;
      Update buffer $\mathcal{B}$ with samples x_N.
    else
      $x_N \sim \mathcal{B}_{\text{MCMC}}$, $\tau^{(1)} \sim \overleftarrow{p}_\varphi^{\otimes N}(\tau \mid x_N)$, $\tau^{(1)} = x_{0:N}$;
      $\tau^{(j)} \sim \overrightarrow{p}_\theta^{\otimes N}(\tau|x_0)$ for $2 \leq j \leq K_{\text{traj}}$.
    end if
    Update θ using $\nabla_\theta \text{Var}_j \left(\log \frac{\overrightarrow{p}_\theta^{\otimes N}(\tau^{(j)}|x_0^{(j)})}{\overleftarrow{p}_\varphi^{\otimes N}(\tau^{(j)}|x_N^{(j)})} - \log p_N(x_N^{(j)}) \right)$
  end while
end for

configurations we considered. We ran 128 chains in parallel, with each chain running 2000 steps for burn-in followed by 25600 steps to collect 128 samples (1 sample every 200 steps), resulting in $128 \times 128 = 16384$ samples.

Masked Diffusion Neural Sampler (MDNS). We adopt the same architecture as in the original MDNS paper, a vision transformer with rotary positional embedding (Heo et al., 2024). We use 2 blocks with 64-dimensional embeddings and 4 attention heads for the Ising model, while we increase the embedding dimension to 128 for the Potts model. Note that the model we used is smaller than the one in the original MDNS paper (4 or 6 blocks), but we found that the smaller model is sufficient for our purpose.

We use weighted denoising cross-entropy (WDCE) loss for MDNS, which is the default option for Ising and Potts models in their paper (see Section 3.3 Zhu et al. (2025)). Since their algorithm with WDCE reuses a batch of samples for multiple gradient steps, we set the batch size as 256 and the number of epochs as 50000, ensuring the number of function evaluations is comparable to ours. Additionally, while the MDNS paper utilised a "warm-up" phase involving pre-training with a tempered target for a fixed number of epochs, we adopt the same annealing schedule as in our methods (see §E.1.1), which we found to be more effective.

D.1.3 Evaluation metrics

This section introduces evaluation metrics for discrete diffusion samplers. We use three target-agnostic evaluation metrics – evidence lower bound (ELBO), evidence upper bound (EUBO; Blessing et al., 2024), and Sinkhorn – as well as two target-specific metrics – magnetisation error and 2-point correlation error. For all metrics, we use $M_{\text{eval}} = 16384$ evaluation samples. Note that EUBO, Sinkhorn, and 2-point correlation error require samples from target distributions, which we obtained from a sufficiently long run of the Swendsen-Wang algorithm; 2^{16} burn-in steps followed by 2^{24} steps (collect a sample every 2^{10} steps).

ELBO. Consider the reverse KL divergence between $p_0 \otimes \overrightarrow{p}_\theta^{\otimes N}$ and $p_{\text{target}} \otimes \overleftarrow{p}^{\otimes N}$:

$$\begin{aligned}
&\mathrm{KL}\left(p_0 \otimes \overrightarrow{p}_\theta^{\otimes N} \,\|\, p_{\text{target}} \otimes \overleftarrow{p}^{\otimes N}\right) \\
&\qquad = \mathop{\mathbb{E}}_{X_{0:N} \sim p_0 \otimes \overrightarrow{p}_\theta^{\otimes N}} \left[\log \frac{p_0 \otimes \overrightarrow{p}_\theta^{\otimes N}(X_{0:N})}{p_{\text{target}} \otimes \overleftarrow{p}^{\otimes N}(X_{0:N})}\right] = -\underbrace{\mathop{\mathbb{E}}_{X_{0:N} \sim p_0 \otimes \overrightarrow{p}_\theta^{\otimes N}} [\log w]}_{=:\text{ELBO}} + \log Z,
\end{aligned}$$

where w is defined in (7). Due to the non-negativity of the KL divergence, ELBO gives a lower bound on $\log Z$. We approximate ELBO by M_{eval} samples.

EUBO. Similar to ELBO, consider the forward KL divergence between $p_{\text{target}} \otimes \overleftarrow{p}^{\otimes N}$ and $p_0 \otimes \overrightarrow{p}_\theta^{\otimes N}$:

$$\begin{aligned}
&\mathrm{KL}\left(p_{\text{target}} \otimes \overleftarrow{p}^{\otimes N} \,\|\, p_0 \otimes \overrightarrow{p}_\theta^{\otimes N}\right) \\
&\qquad = \mathop{\mathbb{E}}_{X_{0:N} \sim p_{\text{target}} \otimes \overleftarrow{p}^{\otimes N}} \left[\log \frac{p_{\text{target}} \otimes \overleftarrow{p}^{\otimes N}(X_{0:N})}{p_0 \otimes \overrightarrow{p}_\theta^{\otimes N}(X_{0:N})}\right] = \underbrace{\mathop{\mathbb{E}}_{X_{0:N} \sim p_{\text{target}} \otimes \overleftarrow{p}^{\otimes N}} [\log w]}_{=:\text{EUBO}} - \log Z.
\end{aligned}$$

EUBO gives an upper bound on $\log Z$. Note that EUBO requires true samples from p_{target}. Again, we use a Monte Carlo estimate with M_{eval} samples. Blessing et al. (2024) suggested EUBO as a metric for measuring mode coverage.

Sinkhorn distance. Sinkhorn distance measures an entropy-regularised optimal transport cost between two distributions. We use Hamming distance as our distance metric, and the regularisation parameter 0.001. We use M_{eval}

Sinkhorn distance. The Sinkhorn distance (Cuturi, 2013) measures the entropy-regularised optimal transport cost between two distributions. We employ the Hamming distance as a distance metric and set the regularisation parameter to 0.001. We compute the distance using two sets of M_{eval} samples, drawn from the target distribution and our model $\overrightarrow{p}$, respectively.

Ising Magnetisation. The state space for the Ising model is $\mathcal{S} = \{-1, 1\}^{L \times L}$. We compute the metrics with respect to some sampling distribution of the spins, π. The magnetisation of a spin i is defined as $M(i) = \mathbb{E}_{x \sim \pi}[x_i]$. We define the average magnetisation of the rows and columns as

$$M^{\text{row}}(k) = \frac{1}{L} \sum_{i \in \text{row}(k)} M(i), \qquad M^{\text{col}}(k) = \frac{1}{L} \sum_{i \in \text{col}(k)} M(i),$$

where $\text{row}(k)$ and $\text{col}(k)$ denote sets of indices corresponding to the spins in row k and column k respectively. We then define the magnetisation error as

$$M_{\text{error}} = \frac{1}{2L} \sum_{k=1}^{L} |M^{\text{row}}(k) - M^{\text{row}}_{\text{true}}(k)| + |M^{\text{col}}(k) - M^{\text{col}}_{\text{true}}(k)|$$

Ising 2-point correlation. The 2-point correlation of two spins, i, j on the lattice is given by $C(i, j) = \mathbb{E}_{x \sim \pi}[x_i x_j] - \mathbb{E}_{x \sim \pi}[x_i]\mathbb{E}_{x \sim \pi}[x_j]$. In a similar fashion to the above row magnetisation, we average all row/column correlations at a distance r along the corresponding dimension,

$$C^{\text{row}}(r) = \frac{1}{L^2} \sum_{k=1}^{L} \sum_{\substack{i \in \text{row}(k) \\ j \in \text{row}((k+r) \mod L) \\ i,j \text{ same column}}} C(i, j), \qquad C^{\text{col}}(r) = \frac{1}{L^2} \sum_{k=1}^{L} \sum_{\substack{i \in \text{col}(k) \\ j \in \text{col}((k+r) \mod L) \\ i,j \text{ same row}}} C(i, j).$$

We then define the two-point correlation error as

$$\frac{1}{2L} \sum_{r=0}^{L-1} |C^{\text{row}}(r) - C^{\text{row}}_{\text{true}}(r)| + |C^{\text{col}}(r) - C^{\text{col}}_{\text{true}}(r)|.$$

Potts magnetisation. Recall the Potts model state space $\mathcal{S} = \{1, \ldots, q\}^{L \times L}$. The Potts magnetisation calculated for a batch B of samples is defined as

$$M(i) = \frac{q \max_{1 \leq c \leq q} (\mu_c^i / |B|) - 1}{q - 1},$$

where $\mu_c^i = \sum_{x \in B} \mathbf{1}_{x_i = c}$ is the number of samples in the batch for which spin i has value c. The values for row/column magnetisation and the magnetisation error are identical to those described in the Ising model, but with the above definition of magnetisation substituted in.

Potts 2-point correlation. The 2-point correlation of the Potts model is defined as

$$C(i, j) = \mathbb{E}\left[\mathbf{1}_{x_i = x_j} - \frac{1}{q}\right].$$

Again, the definitions of average row/column correlation and 2-point correlation error are identical to the Ising model but with the above definition of 2-point correlation substituted in.

D.1.4 Algorithm details, model architectures, and hyperparameters

We employ multiple unmasking (see the last paragraph of §2.1 and §B.1) with $K_{\min} = K_{\max} = 4$, *i.e.*, our forward kernel $\overrightarrow{p}$ unmasks 4 elements at each step, while we use single-step unmasking for evaluation. We adopt the Swendsen-Wang algorithm (Swendsen & Wang, 1986; 1987) for off-policy MCMC exploration. We use the same ViT architecture with a rotary position embedding as MDNS, which is described in §D.1.2, and AdamW (Loshchilov & Hutter, 2019) as optimiser. Table 3 shows the hyperparameters we used for the Ising and Potts experiments.

Table 3: Hyperparameter settings for Ising and Potts model experiments.

	Ising ($L = 16$)	Potts ($L = 16$)
Model type	ViT	
Number of blocks	2	
Number of attention heads	4	
Embedding dim	64	128
Learning rate	1e-3	
Number of training epochs (N_{epochs})	20000	
Batch size (M)	128	
Buffer size	12800	
Off-to-On ratio (R)	2	
MCMC sample ratio (r)	0.2	
MCMC interval (I)	500	
MCMC steps (incl. burn-in) (L)	100	

D.2 SYNTHETIC TARGETS

D.2.1 TARGETS

We define the discrete synthetic target densities as discretisations of continuous distributions using Gray codes (Gray, 1953).

Gray-code discretisation. To discretise a D-dimensional continuous space, we first truncate each dimension to the interval $[-R, R]$, then shift by R and scale by $\frac{1}{2R}$ to map them to $[0, 1]^D$. Each interval is then quantised into integers $\{0, \ldots, 2^b - 1\}$, where b represents the number of quantisation bits. The specific parameters for each target are provided below. In order to transform each bin into a (higher-dimensional) binary variable, we use Gray codes. Gray code orders binary numbers in such a way that two values which are consecutive in the original discretised space only differ by a single bit in Gray code. An example is given in Table 4. For D-dimensional space with b quantisation bits, the dimension of the resulting discrete space is $d = D * b$.

Table 4: Conversion from decimal to Gray code ($b = 3$).

Decimal	Gray
0	000
1	001
2	011
3	010
4	110
5	111
6	101
7	100

Given the energy function $\widetilde{\mathcal{E}}$ defined in $\mathbb{R}^D$, we define the energy $\mathcal{E}$ in gray-coded discrete space $\{0, 1\}^d$ as follows:

$$\mathcal{E}(x) = \widetilde{\mathcal{E}}\left((\texttt{InverseGray}(x) + 0.5) * 2R - R\right) - D \log \frac{R}{2^{b-1}},$$

where $x \in \{0, 1\}^d$ is a binary vector, `InverseGray` is the inverse mapping of Gray code. We add 0.5 to shift the integer values from `InverseGray` and undo the scaling and shifting. The last term is to account for the size of the bin.

We consider two targets, *40GMM* and *ManyWell*, which are common synthetic benchmarks for continuous sampling:

- **40GMM** ($D \in \{2, 4\} \mid R = 50 \mid b = 8$) (Midgley et al., 2023) is a uniform mixture of 40 Gaussians in $\mathbb{R}^D$, where each mixture component has mean $c_i \in \mathbb{R}^D$ and identity covariance I. Each dimension of the c_i are sampled from the uniform distribution $\mathcal{U}[a, b]$ where the upper and lower bounds were chosen so that the resulting Gaussian mixture has small probability density outside the truncation region, $a = -R+3 = -47$ and $b = -R+S-3 = 47$. The energy function of the 40GMM in the continuous space is given by:

$$\widetilde{\mathcal{E}}_{\text{40GMM}}(\tilde{x}) = -\frac{1}{40} \sum_{i=1}^{40} \log p_{\mathcal{N}}(\tilde{x}; c_i, I),$$

  where $\tilde{x} \in \mathbb{R}^D$ and $p_{\mathcal{N}}(\cdot; c, I)$ is the density function of the normal distribution with mean c and covariance I.

- **ManyWell** ($D \in \{4, 10\} \mid R = 4 \mid b = 8$) (Noé et al., 2019; Nüsken & Richter, 2021) is a product of $D/2$ identical DoubleWell distributions and $D/2$ standard Gaussian distributions. The DoubleWell energy is given by:

$$\widetilde{\mathcal{E}}_{\text{DoubleWell}}(\tilde{x}_1) = \tilde{x}_1^4 - 6\tilde{x}_1^2 - 0.5\tilde{x}_1.$$

  where $\tilde{x}_1 \in \mathbb{R}$. Then, the ManyWell energy is defined as:

$$\widetilde{\mathcal{E}}_{\text{ManyWell}}(\tilde{x}) = \sum_{i=1}^{D/2} \widetilde{\mathcal{E}}_{\text{DoubleWell}}(\tilde{x}_{2i}) + \frac{1}{2}\tilde{x}_{2i+1}^2,$$

  where $\tilde{x} \in \mathbb{R}^D$. We use rejection sampling to generate ground-truth samples.

  To make the problem more challenging, we consider a variation called "Rotated" ManyWell, where we rotate each pair of dimensions (x_{2i}, x_{2i+1}) by $\pi/4$, introducing dependencies between them. The energy function of the Rotated ManyWell is defined as

$$\widetilde{\mathcal{E}}_{\text{RotatedManyWell}}(\tilde{x}) = \sum_{i=1}^{D/2} \widetilde{\mathcal{E}}_{\text{DoubleWell}}\left(\frac{\tilde{x}_{2i} + \tilde{x}_{2i+1}}{\sqrt{2}}\right) + \frac{-\tilde{x}_{2i} + \tilde{x}_{2i+1}}{2\sqrt{2}}.$$

We adopt the Rotated ManyWell as the default benchmark throughout the paper.

D.2.2 BASELINES

We consider the same baselines as our experiments on the Ising and Potts models, which are detailed in §D.1.2. For the MH baseline, we use the same hyperparameters as described in §D.1.2, except that we tune H of the Hamming-ball proposal over $\{1, 2, 5, 10\}$ and choose to use $H = 5$, which yields the best average rank of MMD over the four benchmarks that we consider. For MDNS, we use the same MLP architecture as our LV or TB algorithms, while using a larger batch size (256) and a larger number of epochs (50000) to make the number of function evaluations comparable to those of our algorithms.

D.2.3 EVALUATION METRICS

For synthetic targets, we also use ELBO, EUBO, and the Sinkhorn distance, as explained in §D.1.3, whereas we measure the Sinkhorn distance in the continuous space using the L_2 distance instead of the Hamming distance. In addition to those, we compute the maximum mean discrepancy (MMD) using a Gaussian kernel, the L_2 distance, and the median heuristic (Gretton et al., 2012), also with $M_{\text{eval}} = 16384$ samples from the target and the model.

D.2.4 ALGORITHM DETAILS, MODEL ARCHITECTURES, AND HYPERPARAMETERS

We use the Metropolis-Hastings with H-Hamming-ball proposal (§D.1.2) with $H = 5$ as our off-policy MCMC exploration method. We use multiple unmasking only for training ManyWell 10D, with $K_{\text{min}} = K_{\text{max}} = 4$. For all learning-based methods, including our TB and LV algorithms and also MDNS, we use a simple multi-layer perceptron (MLP) with a size chosen to be appropriate for the difficulty of the problem, with the AdamW optimiser (Loshchilov & Hutter, 2019). Table 5 shows a set of hyperparameters of our algorithm that we use for the synthetic targets.

Table 5: Hyperparameter settings for experiments with synthetic targets.

	40GMM ($d = 2 \times 8 = 16$)	40GMM ($d = 4 \times 8 = 32$)	ManyWell ($d = 4 \times 8 = 32$)	ManyWell ($d = 10 \times 8 = 80$)
Model type	MLP			
Number of layers	2	4	2	4
Hidden dim	256			
Learning Rate	1e-3			
Number of training epochs (N_{epochs})	20000			
Batch size (M)	128			
Buffer size	12800			
Off-to-On ratio (R)	2			
MCMC sample ratio (r)	0.2			
MCMC Interval (I)	500			
MCMC Steps (incl. burn in) (L)	100			

D.3 DATA-TO-ENERGY SCHRÖDINGER BRIDGES

We conduct experiments on three pairs of distributions: 3GMM and 4GMM, S-Curve and 10GMM, 10GMM and 40GMM. All distributions have spatial dimension $D = 2$, which is discretised using 8-bit Gray code. We use the same neural network for parametrisation of both forward and backward processes. Hyperparameters are given in Table 6.

Table 6: Hyperparameter settings for Schrödinger bridge experiments with synthetic targets.

Model type	MLP
Number of layers	4
Hidden dim	256
Forward process learning rate	1e-4
Backward process learning rate	1e-3
Number of outer SB steps (num_sb_iter)	50
Number of forward steps (num_fwd_iter)	2500
Number of backward steps (num_bwd_iter)	2500
Batch size (M)	256
Buffer size	25600
Off-to-On ratio (R)	10
MCMC sample ratio (r)	0.5
MCMC Steps (incl. burn in) (L)	200

D.4 Outsourced sampling

D.4.1 Algorithm details, model architectures, and hyperparameters

We sample the latent space of a VQ-VAE model, that is trained following the method provided in Hu et al. (2023). The latent space has the dimension 16, and the latent codebook has vocabulary size 8. To model the posterior, we train a classifier, which is applied to the output of the decoder. The classifier is parameterised by a simple convolutional neural network. For on-policy training we use Log Variance divergence, and for off-policy training we additionally use a replay buffer with MCMC. The neural network is learnt with the AdamW optimiser (Loshchilov & Hutter, 2019). Table 7 shows the hyperparameters used for training the discrete outsourced diffusion sampler.

Table 7: Hyperparameter settings for outsourced sampling experiments.

	MLP	ViT
Number of blocks	-	4
Number of attention heads	-	4
Hidden dim	256	64
Learning rate	1e-3	
Number of epochs (N_{epoch})	20000	
Batch size (M)	256	
Buffer size	25600	
Off-to-On ratio (R)	2	
MCMC Sample ratio (r)	0.5	
MCMC Refresh Interval (I)	10	
MCMC steps (incl. burn-in) (L)	201	

D.4.2 MCMC algorithm

In outsourced experiments on the MNIST dataset the latent space of a generator is a discrete space $\mathcal{S} = \{1, \dots, C\}^d$ with. $C = 8$. For this case we use a a specific MCMC which we denote *Categorical MCMC*. This MCMC algorithm can be viewed as an generalisation of *Hamming ball MCMC*, and it uses the following transition kernel, which is independent over entries x_i:

$$\mathcal{P}(x_i' = c' \mid x_i = c) = \begin{cases} p & c' = c, \\ \frac{1-p}{C-1} & c' \neq c. \end{cases}$$

E Additional experimental results

E.1 Analysis

In the following subsections, we analyse some of the key algorithmic design choices of our off-policy training method, mainly under the setting of sampling in synthetic and Ising/Potts models.

E.1.1 Ablation study on temperature-annealed training

Annealing the temperature of the target distribution throughout the training procedure has been adopted in several works in continuous diffusion samplers (Rissanen et al., 2025; Schopmans & Friederich, 2025; Akhound-Sadegh et al., 2025) and also in discrete diffusion samplers Holderrieth et al. (2025); Zhu et al. (2025), showing powerful empirical gain over non-annealed training. We also adopt a simple temperature annealing scheme for all the learning-based algorithms, where we linearly anneal the inverse temperature from 0 to 1 over half of the training epochs.

Table 8 shows the results from each algorithm with and without the temperature annealing scheme. We observe that temperature annealing provides a consistent performance gain, as expected, while the off-policy training with MCMC exploration is less sensitive to the annealing scheme, especially in the 16×16 Ising where the MCMC algorithm mixes the modes well.

E.1.2 Effect of off-policy to on-policy ratio R

Here, we investigate the impact of the off-policy to on-policy training ratio R. While Algorithm 1 illustrates the procedure for $R \geq 1$, we can easily modify it to handle the case of $R < 1$ such that the ratio between off-policy and on-policy training is R.

Fig. 5 demonstrates the effect of R on the performance of off-policy training for 40GMM ($d = 4 \times 8 = 32$), ManyWell ($d = 10 \times 8 = 80$), and the 16×16 Ising model with $\beta = 0.6$. In general, increasing R improves EUBO but degrades ELBO. We find that values of R between 1 and 4 offer a reasonable balance.

Table 8: Ablation study on temperature-annealed training (mean±std over 5 runs).

Target →	40GMM (d = 4)				ManyWell (d = 10)				16 × 16 Ising (β = 0.6)				
Method ↓ Metric →	ELBO ↑	EUBO ↓	MMD ↓	Sink. ↓	ELBO ↑	EUBO ↓	MMD ↓	Sink. ↓	ELBO ↑	EUBO ↓	Sink. ↓	Mag. ↓	Corr. ↓
MDNS													
w/o annealing	-3.54±0.26	91.54±12.60	0.58±0.13	3508.04±1328.10	41.20±0.97	54.19±0.11	0.04±0.01	1.83±0.04	309.78±0.00	403.55±30.68	117.99±1.22	0.97±0.00	0.95±0.00
w/ annealing	-16.66±2.25	14.02±1.50	0.17±0.04	349.31±69.18	41.52±0.65	54.16±0.14	0.04±0.01	1.82±0.05	310.18±0.33	341.82±38.37	48.71±55.25	0.41±0.46	0.38±0.46
LV (on-policy)													
w/o annealing	-3.71±0.00	122.12±6.96	0.59±0.06	3593.82±551.92	48.79±0.02	67.20±0.83	0.33±0.01	4.81±0.20	309.78±0.02	388.39±16.48	116.25±2.23	0.97±0.00	0.95±0.00
w/ annealing	-2.56±0.27	77.96±13.03	0.42±0.09	2265.84±685.58	49.10±0.04	57.40±0.26	0.14±0.01	1.34±0.02	309.77±0.04	422.53±94.60	116.96±2.15	0.97±0.00	0.95±0.00
LV + Buffer													
w/o annealing	-3.51±0.39	91.12±7.66	0.56±0.06	3322.93±744.78	45.17±0.21	54.17±0.06	0.05±0.01	1.79±0.04	309.79±0.00	373.49±8.86	117.54±1.83	0.97±0.00	0.95±0.00
w/ annealing	-2.68±0.19	49.77±11.95	0.38±0.10	1566.19±596.76	44.83±0.41	54.29±0.08	0.05±0.01	1.83±0.07	308.55±1.36	311.05±0.36	4.33±0.53	0.40±0.30	0.27±0.25
LV + Buffer + MCMC													
w/o annealing	-4.43±2.99	45.64±18.31	0.48±0.15	2215.06±1149.08	43.79±0.50	54.19±0.11	0.06±0.01	1.97±0.06	308.15±1.17	311.21±0.32	4.35±0.39	0.37±0.24	0.21±0.17
w/ annealing	-13.41±6.37	13.89±1.30	0.57±0.05	1241.69±490.85	42.50±0.31	54.44±0.02	0.07±0.01	2.16±0.03	310.18±0.24	310.65±0.08	3.85±0.20	0.14±0.13	0.04±0.05
TB (on-policy)													
w/o annealing	-3.71±0.00	115.00±5.64	0.55±0.03	3219.80±587.75	48.75±0.04	68.14±2.13	0.32±0.02	4.84±0.30	307.64±0.87	2607.94±855.53	127.07±1.45	1.00±0.01	0.95±0.00
w/ annealing	-2.47±0.30	71.53±7.55	0.40±0.07	2142.65±637.28	49.05±0.05	57.48±0.28	0.15±0.02	1.37±0.02	309.79±0.00	377.92±14.19	117.22±0.68	0.97±0.00	0.95±0.00
TB + Buffer													
w/o annealing	-3.40±0.39	91.66±13.17	0.56±0.04	3391.08±364.60	48.66±0.19	53.31±0.14	0.04±0.01	1.33±0.02	309.78±0.00	371.93±12.93	117.26±1.67	0.97±0.00	0.95±0.00
w/ annealing	-5.97±1.06	4.20±1.39	0.07±0.03	114.11±53.48	48.79±0.07	53.18±0.03	0.03±0.01	1.30±0.01	310.42±0.03	310.56±0.01	3.59±0.04	0.04±0.02	0.00±0.00
TB + Buffer + MCMC													
w/o annealing	-3.05±0.52	52.65±12.13	0.41±0.12	1993.90±732.09	48.78±0.14	53.04±0.04	0.03±0.01	1.30±0.02	310.36±0.07	310.60±0.03	3.51±0.05	0.06±0.03	0.00±0.00
w/ annealing	-7.04±0.88	1.20±0.21	0.05±0.01	9.24±4.33	48.73±0.18	52.86±0.03	0.04±0.01	1.36±0.02	310.43±0.01	310.55±0.01	3.47±0.12	0.02±0.01	0.00±0.00

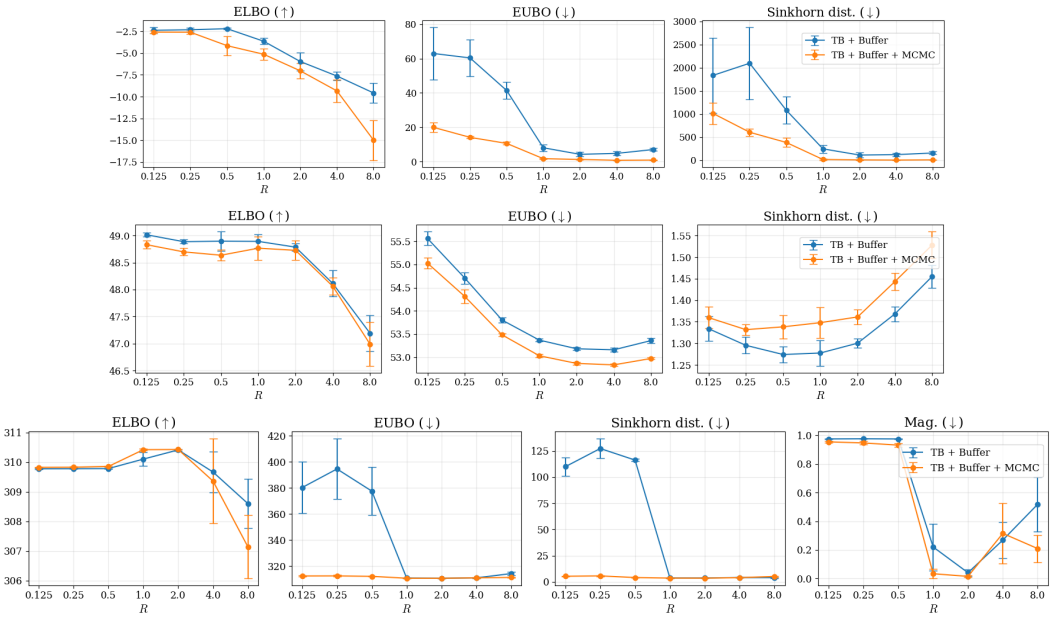

Figure 5: Effect of off-policy to on-policy ratio R in 40GMM ($d = 4 \times 8 = 32$, top), ManyWell ($d = 10 \times 8 = 80$, mid), and 16×16 Ising ($\beta = 0.6$, bottom). The error bars show a 1-std range from 5 runs.

E.1.3 Effect of MCMC algorithms for Ising and Potts

We use Swendsen-Wang (Swendsen & Wang, 1986; 1987) MCMC, a specialised MCMC algorithm for Ising and Potts models, for off-policy exploration. Here, we replace the Swendsen-Wang with Metropolis-Hastings (MH) with 1-Hamming-ball proposal. Table 9 shows the results.

Table 9: Effect of MCMC Algorithms on Ising and Potts models (mean±std over 5 runs).

Target →	16 × 16 Ising (β = 0.4407)			16 × 16 Ising (β = 0.6)			16 × 16 Ising (β = 1.2)			16 × 16 Potts (β = 1.005)			16 × 16 Potts (β = 1.2)		
Method ↓ Metric →	Sink. ↓	Mag. ↓	Corr. ↓	Sink. ↓	Mag. ↓	Corr. ↓	Sink. ↓	Mag. ↓	Corr. ↓	Sink. ↓	Mag. ↓	Corr. ↓	Sink. ↓	Mag. ↓	Corr. ↓
MDNS	61.60±18.23	0.32±0.35	0.23±0.26	48.71±55.25	0.41±0.46	0.38±0.46	126.27±0.90	1.00±0.00	1.00±0.00	84.78±10.15	0.08±0.06	0.01±0.00	99.95±70.52	0.58±0.46	0.01±0.00
LV + Buffer															
+ MH MCMC	59.47±1.81	0.06±0.06	0.03±0.02	8.24±4.28	0.45±0.27	0.27±0.34	71.08±57.89	1.00±0.00	0.99±0.01	81.74±5.32	0.12±0.16	0.03±0.02	66.73±37.51	0.95±0.00	0.00±0.00
+ Swendsen-Wang	47.34±0.90	0.12±0.07	0.06±0.01	3.85±0.20	0.14±0.13	0.04±0.05	0.04±0.04	0.05±0.08	0.01±0.02	84.58±1.02	0.04±0.03	0.09±0.02	19.56±5.21	0.13±0.10	0.02±0.02
TB + Buffer															
+ MH MCMC	59.45±1.58	0.05±0.04	0.03±0.02	6.38±0.37	0.14±0.19	0.07±0.11	51.24±61.74	1.00±0.00	0.99±0.01	78.40±0.48	0.04±0.02	0.02±0.01	84.24±55.93	0.68±0.32	0.00±0.00
+ Swendsen-Wang	46.22±0.36	0.04±0.02	0.02±0.01	3.47±0.12	0.02±0.01	0.00±0.00	0.02±0.00	0.03±0.01	0.00±0.00	78.50±0.83	0.03±0.02	0.01±0.01	12.37±0.82	0.03±0.02	0.00±0.00

E.2 VISUALISATIONS

Here we provide additional visualisation of samples in addition to the ones in the main text.

E.2.1 ISING AND POTTS MODEL

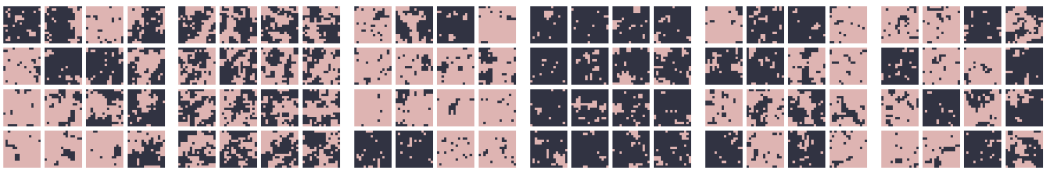

Figure 6: Visualisation of 16 samples generated by each method for the 16×16 Ising model with $\beta = 0.4407$. The samples are obtained from the first run (seed 0).

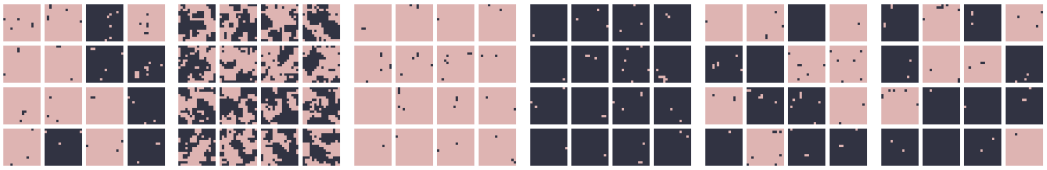

Figure 7: Visualisation of 16 samples generated by each method for the 16×16 Ising model with $\beta = 0.6$. The samples are obtained from the first run (seed 0).

E.2.2 DISCRETISED SYNTHETIC DENSITIES

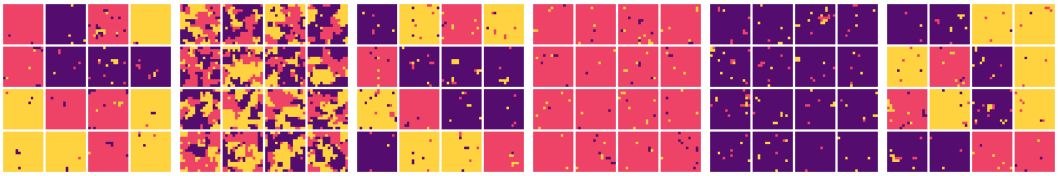

Ground Truth | MH | MDNS | TB (on-policy) | TB + Buffer | TB + Buffer + MCMC

Figure 8: Samples generated by each method for the 16×16 Potts model with $\beta = 1.2$, $q = 3$.

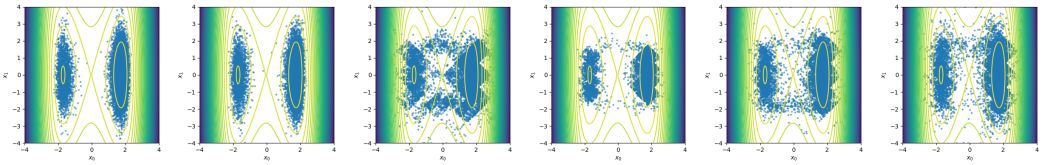

Ground Truth | MH | MDNS | TB (on-policy) | TB + Buffer | TB + Buffer + MCMC

Figure 9: Visualisation of samples generated by each method for the discretised ManyWell ($d = 10 \times 8 = 80$). The samples are obtained from the first run (seed=0) and projected to the first two dimensions.

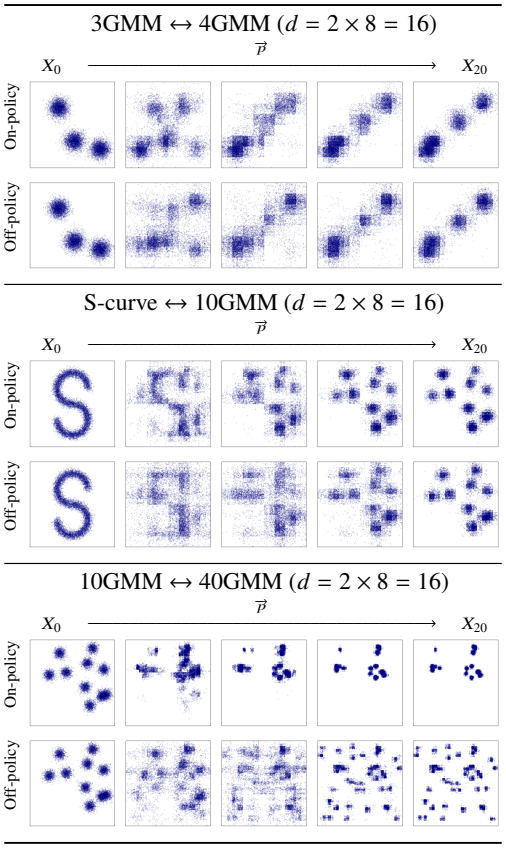

Figure 10: Comparison of discrete-space Schrödinger bridges on 16-dimensional binary Gray-coded spatial data learnt by data-to-energy IPF with on-policy and off-policy LV training.

E.2.3 Outsourced discrete diffusion sampling experiments on MNIST

Ones Fives Sevens Odd Even

Figure 11: Visualisations of decoded samplers of a discrete diffusion sampler in latent space of a VQ-VAE trained on MNIST. The diffusion sampler is parameterised by MLP model, on-policy method (LV) is used for training.

Ones Fives Sevens Odd Even

Figure 12: Visualisations of decoded samplers of a discrete diffusion sampler in latent space of a VQ-VAE trained on MNIST. The diffusion sampler is parameterised by MLP model, off-policy method (LV + Buffer + MCMC) is used for training.

Ones Fives Sevens Odd Even

Figure 13: Visualisations of decoded samplers of a discrete diffusion sampler in latent space of a VQ-VAE trained on MNIST. The diffusion sampler is parameterised by ViT model, on-policy method (LV) is used for training.

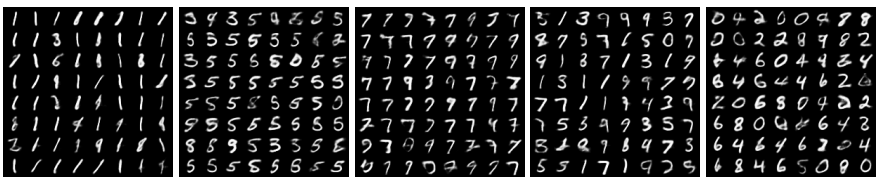

Ones Fives Sevens Odd Even

Figure 14: Visualisations of decoded samplers of a discrete diffusion sampler in latent space of a VQ-VAE trained on MNIST. The diffusion sampler is parameterised by ViT model, off-policy method (LV + Buffer + MCMC) is used for training.